



DEGREE PROJECT IN THE BUILT ENVIRONMENT,  
SECOND CYCLE, 30 CREDITS  
*STOCKHOLM, SWEDEN 2016*

# **Detection and Analysis of GNSS Multipath**

**SHINAN WANG**

**KTH ROYAL INSTITUTE OF TECHNOLOGY  
SCHOOL OF ARCHITECTURE AND THE BUILT ENVIRONMENT**

## Abstract

Multipath effect is generated when a signal arrives at the antenna by multiple paths instead of one direct path. It is, to a large extent, dependent on the surrounding environment of the antenna and the satellite geometry. Despite all the efforts put into the mitigation of multipath errors, it remains the dominant error source that cannot be ignored for GNSS precise positioning and other GNSS applications. In this thesis report, two methods have been developed with Trimble Business Center and MATLAB to study the presence and performance of multipath effect. The first method – Trimble baseline analysis focuses on the height change pattern of the study station with regard to its reference station over time. The second method – RINEX analysis focuses on the change of the geometry-free combination of pseudorange codes ( $R_{p2} - R_{p1}$ ) and carrier phase measurements ( $\varphi_{L1} - \varphi_{L2}$ ) over time. These two methods have been firstly tested on station KTH and then applied on station Vidsel and station Botsmark. Various forms of results all indicate the existence of multipath effect on the three suspicious stations. The height value of the study station has a variation pattern on a daily basis because of multipath. Multipath errors also cause noise in the satellite signals, with pseudorange more affected than carrier phase. It is also worth-noted that satellite at low elevation angle is more susceptible to multipath errors than that at high elevation angle.

## Sammanfattning

Flervägsfel genereras när en signal anländer till antennen genom flera olika vägar i stället för den direkta vägen från satelliten. Det är i stor utsträckning beroende på den omgivande miljön av antennen och satellitgeometrin. Trots olika metoder för att reducera flervägsfel, är det fortfarande en dominerande felkälla som inte kan ignoreras för precis positionering med GNSS och andra GNSS-tillämpningar. I denna rapport har två metoder utvecklats med Trimble Business Center och MATLAB för att studera närvaron och effekten av flervägsfelet. Den första metoden - Trimble baslinje analys fokuserar på förändring i höjden för studie stationen relativt till referensstationen över tid. Den andra metoden - RINEX analys fokuserar på förändring av den geometriska kombination av pseudoavståndsmätningar ( $R_{p2} - R_{p1}$ ) och fasmätningar ( $\varphi_{L1} - \varphi_{L2}$ ) över tid. Dessa två metoder har först testats på KTH-stationen och sedan appliceras på stationen Vidsel och stationen Botsmark. Olika resultat indikerar förekomsten av flervägsfel på de tre stationer. Höjden för studiestationerna har ett dagligt variationsmönster på grund av flervägsfelet. Flervägsfel orsakar även buller i satellitsignalerna, var pseudoavstånd är mer drabbade än fasmätningarna. Det är också värt att notera att satelliter med låg elevationsvinkel är mer mottagliga för flervägsfel än vid hög elevationsvinkel.

## **Acknowledgement**

To my supervisor, Anna B. O. Jensen, your advice and feedback throughout this process have been invaluable. This thesis would not have been possible without your consistent support for the past several months. To my teacher, Milan Horemuz, your support for software installation and data collection is vital for this thesis work.

I would like to send my gratitude to Lanmåteriet, who provided me the GNSS data and sent me information regarding the two SWEPOS stations up in the north of Sweden.

And to my family and friends, for your love and encouragement, my admiration and appreciation could not be deeper.

# Contents

- 1. Introduction** ..... 1
  - 1.1 Background ..... 1
  - 1.2 Related work ..... 2
    - 1.2.1 Multipath detection..... 2
    - 1.2.2 Multipath mitigation..... 3
  - 1.3 Purpose statement ..... 3
- 2. Method** ..... 4
  - 2.1 Trimble baseline analysis..... 4
    - 2.1.1 Data collection and processing ..... 5
    - 2.1.2 Time series and correlation analyses..... 8
  - 2.2 RINEX analysis..... 9
    - 2.2.1 Theory description..... 9
    - 2.2.2 Data collection, processing and analysis ..... 9
- 3. Experiment and application** .....13
  - 3.1 Experiment with station KTH.....13
    - 3.1.1 Result of Trimble baseline analysis .....13
    - 3.1.2 Result of RINEX analysis .....20
  - 3.2 Application with station Vidsel and station Botsmark .....26
    - 3.2.1 Result of Trimble baseline analysis .....26
    - 3.2.2 Result of RINEX analysis .....31
- 4. Conclusion and future work**.....40
  - 4.1 Conclusion for GNSS multipath effect .....40
  - 4.2 Possible future work .....41
- Reference** .....42

## List of Figures

Figure 1.1 Outdoor multipath effect (Hofmann-Wellenhof et al., 2008). .....	1
Figure 1.2 Effect of multipath on pseudorange code measurement (Axelrad et al., 2005). .....	2
Figure 1.3 Effect of multipath on carrier phase measurement (Axelrad et al., 2005).....	3
Figure 2.1 Workflow for Trimble baseline analysis. ....	4
Figure 2.2 SWEPOS stations and other stations used in positioning services (source: <a href="https://swepos.lantmateriet.se/tjanster/kartstod/kartstod.aspx">https://swepos.lantmateriet.se/tjanster/kartstod/kartstod.aspx</a> ; data accessed: 26 <sup>th</sup> Feb 2016).....	5
Figure 2.3 Import data to TBC.....	6
Figure 2.4 Process data in TBC. ....	7
Figure 2.5 Export data from TBC. ....	8
Figure 2.6 Workflow for RINEX analysis. ....	10
Figure 2.7 Multipath effect on GPS pseudorange and carrier phase observations (source: <a href="http://www.navipedia.net/index.php/File:Multipath_Fig_2.png">http://www.navipedia.net/index.php/File:Multipath_Fig_2.png</a> ; data accessed: 24 <sup>th</sup> Apr 2016).....	11
Figure 2.8 Trimble planning tool. ....	12
Figure 2.9 Illustration for time shift. ....	12
Figure 3.1 Photo for the mounted antenna of station KTH. ....	13
Figure 3.2 Location of station KTH and its reference station Mosebacke (source: <a href="https://swepos.lantmateriet.se/tjanster/kartstod/kartstod.aspx">https://swepos.lantmateriet.se/tjanster/kartstod/kartstod.aspx</a> ; data accessed: 21 <sup>st</sup> Mar 2016).....	14
Figure 3.3 Datasets for 25 <sup>th</sup> Feb and 26 <sup>th</sup> Feb 2016 of station KTH. ....	14
Figure 3.4 First ten-hour of Figure 3.3.....	15
Figure 3.5 Datasets for 17 <sup>th</sup> Feb to 26 <sup>th</sup> Feb 2016 of station KTH. ....	15
Figure 3.6 First five-hour of Figure 3.5. ....	16
Figure 3.7 Ionospheric activity of Svealand on 18 <sup>th</sup> Feb 2016 from SWEPOS ionosphere monitor (source: <a href="https://swepos.lantmateriet.se/tjanster/jonomonitor/jonomonitor.aspx">https://swepos.lantmateriet.se/tjanster/jonomonitor/jonomonitor.aspx</a> ; data accessed: 13 <sup>th</sup> May 2016).....	16
Figure 3.8 Datasets for 17 <sup>th</sup> Feb to 26 <sup>th</sup> Feb 2016 of station KTH, except for 18 <sup>th</sup> Feb and 23 <sup>rd</sup> Feb. ....	17
Figure 3.9 First ten-hour view of Figure 3.8. ....	17

Figure 3.10 Correlation between two datasets. ....	18
Figure 3.11 Missing records for GPS day 55 and 50.....	18
Figure 3.12 Elevation angle and azimuth of satellite G05 for station KTH on 26 <sup>th</sup> Feb 2016. .....	21
Figure 3.13 Multipath effect on pseudorange and carrier phase observations of satellite for station KTH G05 on 26 <sup>th</sup> Feb 2016. ....	21
Figure 3.14 Elevation angle and azimuth of satellite G06 for station KTH on 26 <sup>th</sup> Feb. ...	22
Figure 3.15 Multipath effect on pseudorange and carrier phase observations of satellite G06 for station KTH on 26 <sup>th</sup> Feb 2016. ....	22
Figure 3.16 Elevation angle and azimuth of satellite G15 for station KTH on 26 <sup>th</sup> Feb. ...	23
Figure 3.17 Multipath effect on pseudorange and carrier phase observations of satellite G15 for station KTH on 26 <sup>th</sup> Feb 2016. ....	23
Figure 3.18 Elevation angle and azimuth of satellite G26 for station KTH on 26 <sup>th</sup> Feb. ...	24
Figure 3.19 Multipath effect on pseudorange and carrier phase observations of satellite G26 for station KTH on 26 <sup>th</sup> Feb 2016. ....	24
Figure 3.20 Elevation angle and azimuth of satellite G31 for station KTH on 26 <sup>th</sup> Feb. ...	25
Figure 3.21 Multipath effect on pseudorange and carrier phase observations of satellite G31 for station KTH on 26 <sup>th</sup> Feb 2016. ....	25
Figure 3.22 The surrounding environment of station Vidsel, and the antenna is mounted on the side of the chimney (The photo is provided by Lantmäteriet). ....	26
Figure 3.23 Photo for the mounted antenna of station Botsmark (The photo is provided by Lantmäteriet). ....	27
Figure 3.24 Location of station Vidsel and its reference station Kåbdalis (source: <a href="https://swepos.lantmateriet.se/tjanster/kartstod/kartstod.aspx">https://swepos.lantmateriet.se/tjanster/kartstod/kartstod.aspx</a> ; data accessed: 2 <sup>nd</sup> May 2016).....	27
Figure 3.25 Location of station Botsmark and its reference station Vindelns (source: <a href="https://swepos.lantmateriet.se/tjanster/kartstod/kartstod.aspx">https://swepos.lantmateriet.se/tjanster/kartstod/kartstod.aspx</a> ; data accessed: 2 <sup>nd</sup> May 2016).....	28
Figure 3.26 Datasets for 21 <sup>st</sup> Mar to 25 <sup>th</sup> Mar 2016 of station Vidsel. ....	29
Figure 3.27 First ten-hour of Figure 3.26. ....	29
Figure 3.28 Datasets for 21 <sup>st</sup> Mar to 25 <sup>th</sup> Mar 2016 of station Botsmark. ....	30
Figure 3.29 First ten-hour of Figure 3.28. ....	30
Figure 3.30 Elevation angle and azimuth of satellite G03 for station Vidsel on 25 <sup>th</sup> Mar 2016.....	32

Figure 3.31 Multipath effect on pseudorange and carrier phase observations of satellite G03 for station Vidsel on 25 <sup>th</sup> Mar 2016.....	32
Figure 3.32 Elevation angle and azimuth of satellite G08 for station Vidsel on 25 <sup>th</sup> Mar 2016.....	33
Figure 3.33 Multipath effect on pseudorange and carrier phase observations of satellite G08 for station Vidsel on 25 <sup>th</sup> Mar 2016.....	33
Figure 3.34 Elevation angle and azimuth of satellite G17 for station Vidsel on 25 <sup>th</sup> Mar 2016.....	34
Figure 3.35 Multipath effect on pseudorange and carrier phase observations of satellite G17 for station Vidsel on 25 <sup>th</sup> Mar 2016.....	34
Figure 3.36 Elevation angle and azimuth of satellite G28 for station Vidsel on 25 <sup>th</sup> Mar 2016.....	35
Figure 3.37 Multipath effect on pseudorange and carrier phase observations of satellite G28 for station Vidsel on 25 <sup>th</sup> Mar 2016.....	35
Figure 3.38 Elevation angle and azimuth of satellite G03 for station Botsmark on 25 <sup>th</sup> Mar 2016.....	36
Figure 3.39 Multipath effect on pseudorange and carrier phase observations of satellite G03 for station Botsmark on 25 <sup>th</sup> Mar 2016.....	36
Figure 3.40 Elevation angle and azimuth of satellite G08 for station Botsmark on 25 <sup>th</sup> Mar 2016.....	37
Figure 3.41 Multipath effect on pseudorange and carrier phase observations of satellite G08 for station Botsmark on 25 <sup>th</sup> Mar 2016.....	37
Figure 3.42 Elevation angle and azimuth of satellite G17 for station Botsmark on 25 <sup>th</sup> Mar 2016.....	38
Figure 3.43 Multipath effect on pseudorange and carrier phase observations of satellite G17 for station Botsmark on 25 <sup>th</sup> Mar 2016.....	38
Figure 3.44 Elevation angle and azimuth of satellite G28 for station Botsmark on 25 <sup>th</sup> Mar 2016.....	39
Figure 3.45 Multipath effect on pseudorange and carrier phase observations of satellite G28 for station Botsmark on 25 <sup>th</sup> Mar 2016.....	39

## List of Tables

Table 3.1 Correlation matrix for the 10 datasets of station KTH .....	19
Table 3.2 Correlation matrix for the 5 datasets of station Botsmark .....	29

# 1. Introduction

## 1.1 Background

Multipath describes the situation where signals from the GNSS satellites travel over multiple paths before they arrive at the antenna front end (Jakobsen, 2010). In the outdoor environment can multipath be described as the reflection of satellite signals illustrated in Figure 1.1. The reflection is mainly caused by metal, glass, water, wet leaves, wet ground etc. As displayed in Figure 1.1, the satellite signals arrive at the receiver on two kinds of different paths, direct one and indirect ones (Hofmann-Wellenhof et al., 2008). Since the indirect paths are longer than the direct path, multipath arrivals are delayed compared to the direct one. Multipath reflections from nearby objects can arrive at short delays after the arrival of the direct path, which introduces errors in pseudorange and carrier phase measurements (Kaplan and Hegarty, 2006).

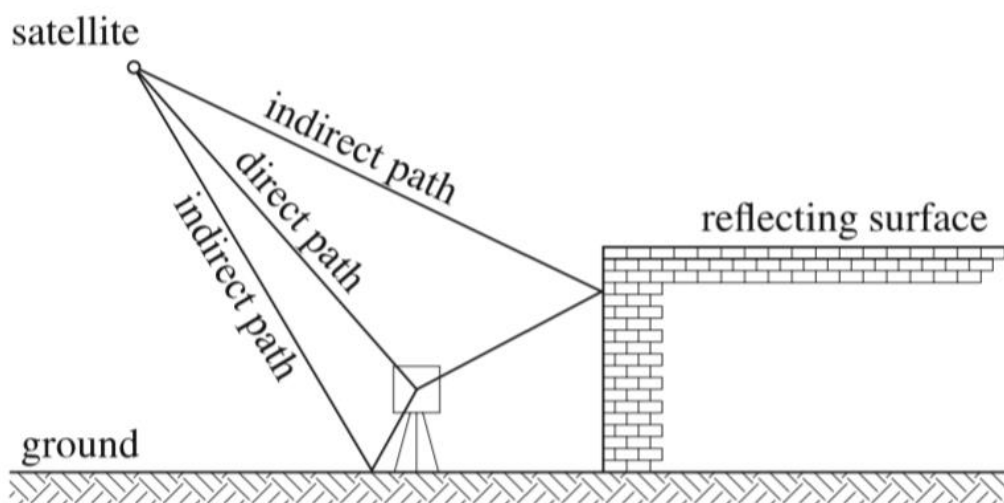


Figure 1.1 Outdoor multipath effect (Hofmann-Wellenhof et al., 2008).

The multipath errors of pseudoranges can be grouped into three classes, diffuse forward scattering from a widely distributed area, specular reflection from well-defined objects or reflective surfaces in the vicinity of the antenna, and fluctuations of very low frequency, usually associated with reflection from the surface of water (Tranquilla and Carr, 1990/91). Therefore, the multipath errors are dependent on the surrounding environment to a large extent. Also these errors are different among the signals from different satellites, and produce errors in position, velocity, and time (Kaplan and Hegarty, 2006). When purely the geometry of satellites is taken into consideration, signals received from satellites of low elevation angle are more susceptible to multipath than signals from satellites of high elevation angles (Hofmann-Wellenhof et al., 2008). The difference between indirect path and direct one is larger for satellites at low elevation than that for satellites at high elevation. It is also worth-noted that pseudoranges are more affected by multipath than carrier phase measurements. In the typical case, multipath error in pseudorange measurement is 1-5m depending on the surroundings and the quality of the receiver. Multipath noise in carrier phase measurements however is limited to a quarter wavelength or in the range of 1-5cm, and it is generally well below 2cm (Axelrad et al., 2005).

As mentioned in the previous paragraph, the multipath effect depends on mainly two factors: the surrounding environment of the GNSS antenna (as well as the type and quality of the antenna) and the satellite geometry. Based on the current GPS orbit design, the entire satellite configuration normally advances roughly 4 minutes between two consecutive days. Thus the positioning measurements derived from the repetition of the GPS satellite constellation between two sidereal days should be influenced by "systematic" multipath (Vázquez B. and Grejner-Brzeziska, 2012). It means that multipath effects are repeated after 23 hours 56 minutes, although the short-term behaviour of multipath appears random. And there ought to be a day-to-day correlation if the environment remains unchanged.

## 1.2 Related work

### 1.2.1 Multipath detection

The presence of multipath can be detected and analysed in several ways. The most complete models for multipath include features of the tracking loops, which are used in a closed loop to follow continuously the code and carrier parameters of the incoming signal (Axelrad et al., 2005). However, it is sufficient to consider the basic model assuming no coupling between the code loops and coherent tracking in this thesis project. For the pseudorange code measurement, Figure 1.2 illustrates the simple model of the direct and indirect signal components. The composite signal has a clear shape change caused by multipath. For the carrier phase measurement, Figure 1.3 displays the simplified model of the effect of multipath. On carrier phase plane, there is an angle between the composite signal and the direct one. Multipath effect on carrier phase measurement is directly related to the signal to noise ratio (SNR). Analyses of multipath can be performed by examining SNR for each satellite and time interval based on simplified mathematical model (Bilich and Larson, 2007).

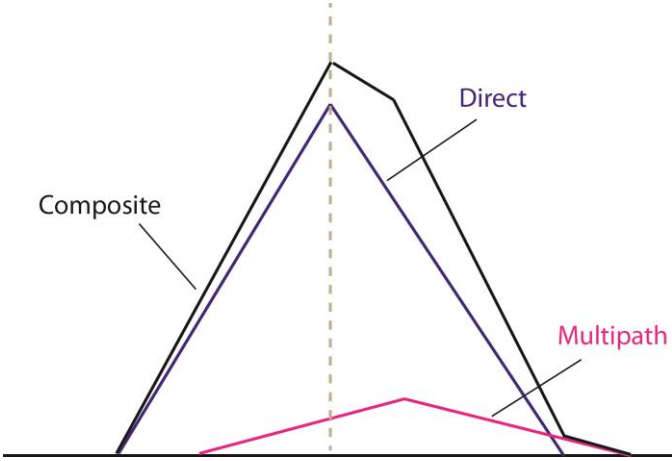


Figure 1.2 Effect of multipath on pseudorange code measurement (Axelrad et al., 2005).

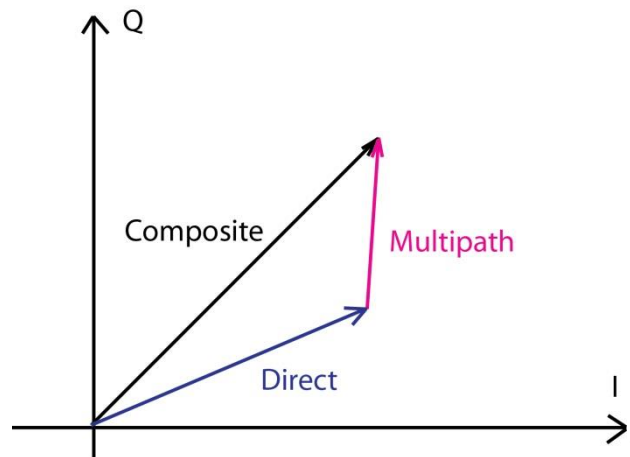


Figure 1.3 Effect of multipath on carrier phase measurement (Axelrad et al., 2005).

### 1.2.2 Multipath mitigation

Various methods have been developed to reduce the multipath errors, and they can be classified into three main categories: antenna-based mitigation, improved receiver technology, and signal and data processing (Ray et al., 1999).

Antenna siting, and removal or modification of reflective structures in the vicinity of the antenna is the most straightforward and also effective method to improve signal quality. Open field is a preferable environment for the antenna location, and placing the antenna closer to the ground can also decrease observed multipath errors (Kaplan and Larson, 2006). Improving the receiver technology for multipath reduction includes narrow correlation spacing, extending the multipath estimation delay lock loop, enhancing the strobe correlator multipath rejection (Hofmann-Wellenhof et al., 2008). There are numerous methods developed for signal and data processing, such as smoothing carrier phases (Lee and Rizos, 2008) and using data combinations (Phelts and Enge, 2000).

All in all, there is a considerable investigation into the development of multipath mitigation techniques. Some of the techniques have been incorporated into production receivers, while others remain research topics.

## 1.3 Purpose statement

Despite all the efforts spent, multipath errors remain the dominant error source for most fixed sites and stations (Axelrad et al., 2005). It is also partly due to the continuous improvements in reducing other error sources. A satisfactory general multipath model is still not available, mainly because of the variant surrounding environment where satellite-reflector-antenna geometry can vary largely (Ata, 2014). Therefore, multipath is an effect that cannot be ignored with the aim of precise positioning, because it leads to positioning errors and reduces position accuracy. Multipath error also has an influence on other applications derived from GNSS observations, including timing (Ray and Senior, 2003), water vapor products (Braun et al., 2001), and seismic waves (Larson et al., 2003). Thus an awareness of the presence of multipath effect and also an understanding of the magnitude of multipath errors is essential.

The thesis project aims at investigating the presence of multipath, examining the daily pattern, and differentiating its effect on pseudorange from carrier phase measurements. In this way, it is expected that users of GNSS signals become more aware of the presence of multipath and also its influence on the signal quality.

## 2. Method

In this thesis project, two methods have been applied to detect the existence of significant multipath and analyse the daily pattern – Trimble baseline analysis and RINEX analysis. Trimble Business Center software (TBC) and MATLAB are the two main tools used.

### 2.1 Trimble baseline analysis

Trimble baseline analysis has been conducted within both TBC and MATLAB. The procedure can be divided into four steps – data collection, processing in TBC, analyses in MATLAB, and conclusion (Figure 2.1). They will be demonstrated in detail in the following two sub-sections.

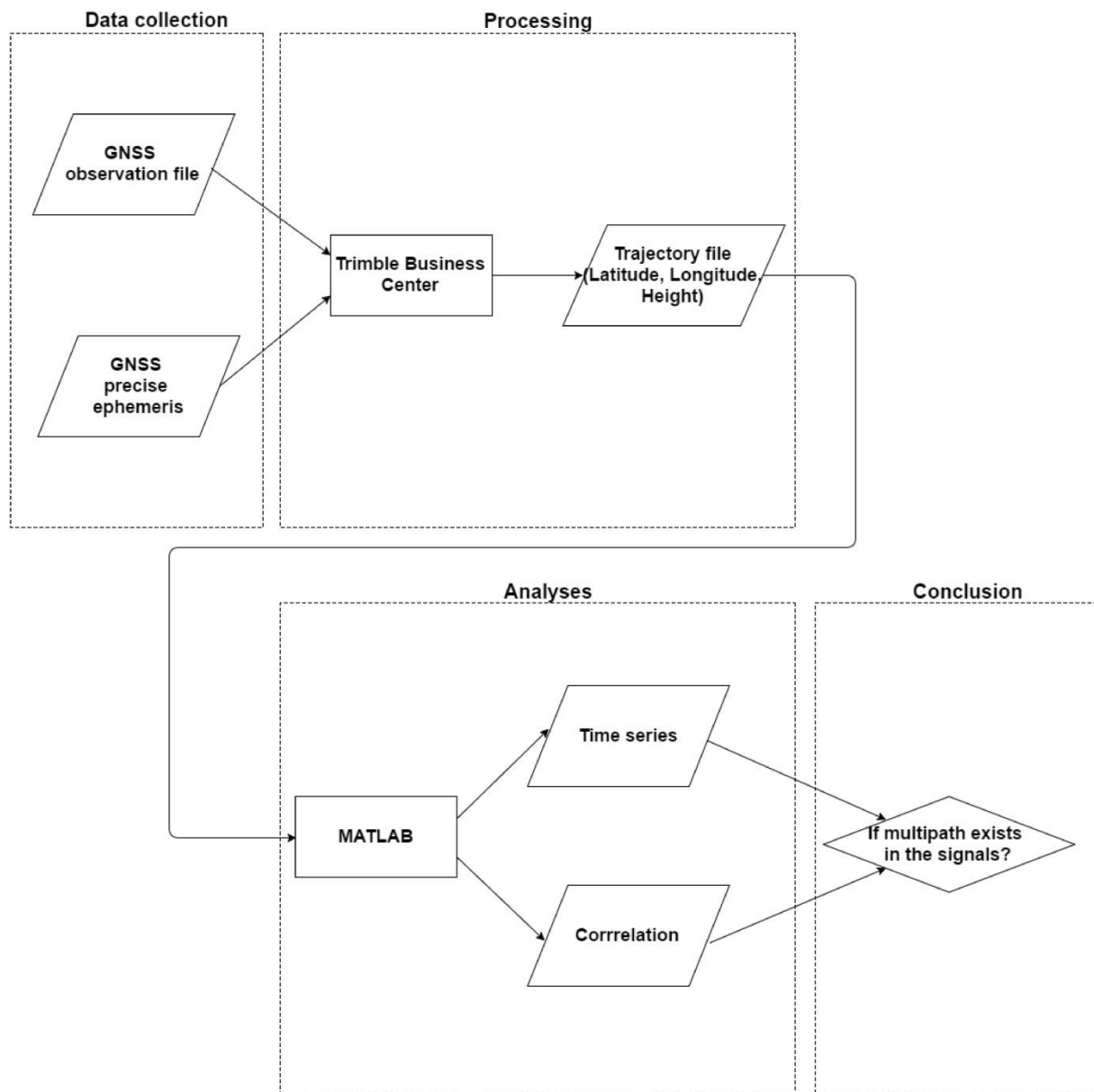


Figure 2.1 Workflow for Trimble baseline analysis.

### 2.1.1 Data collection and processing


The GNSS observation file in the Receiver Independent Exchange Format (RINEX) made available by Lantmäteriet is used. The data files are produced by SWEPOS which is Lantmäteriet's support system for satellite positioning with over 350 reference stations in Sweden (Figure 2.2). Data can be downloaded from Lantmäteriet's ftp server (<ftp://ftp-sweposdata.lm.se/>), and they are listed according to GPS days. According to the GPS calendar (<http://www.ngs.noaa.gov/CORS/Gpscal.shtml>), GPS days can be converted to calendar days. GNSS precise ephemeris processed by the International GNSS Service (IGS) is used for orbit information (Dow et al., 2009). The data can be downloaded via their ftp server (<ftp://ftp.igs.org/pub/product>).



Figure 2.2 SWEPOS stations and other stations used in positioning services (source: <https://swepos.lantmateriet.se/tjanster/kartstod/kartstod.aspx>; data accessed: 26<sup>th</sup> Feb 2016).

The method with two stations (one study station and the other reference station) and two days of data analysed in the Trimble Business Center software is described as the following:

First the RINEX data and precise ephemeris are imported into TBC. The data should be downloaded to the PC first.

1. A new project is created using the Metric template. The coordinate system SWEREF 99, zone 18 00, geoid model SW082000 is selected under Project -> Change Coordinate System.
2. Data from the two stations are imported. It is done under File -> Import data (\*.d: compressed observation data). The coordinate quality of the reference station is marked as Control quality, which is done in the Properties window, that is, in Project Explorer expand the point of the reference station, by right clicking on Global and choose properties and then clicking on the  by the coordinates.
3. GPS precise ephemeris is imported. It is done again under File -> Import data (\*.sp3.Z: compressed precise ephemeris data). This orbit rapid solution is much better than the broadcast ephemeris. Now all the points measured in the field including vectors to the reference station can be seen in Figure 2.3 below.

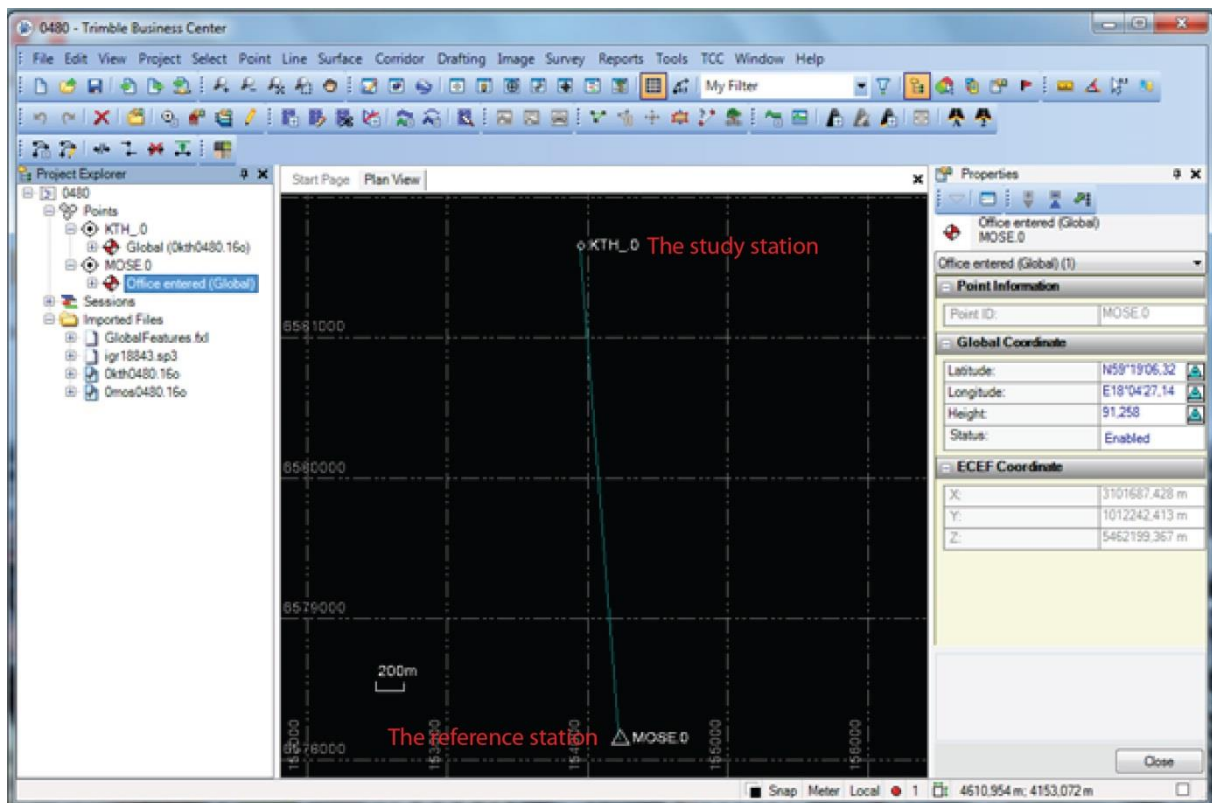


Figure 2.3 Import data to TBC.

The data files are from permanent GNSS stations, so they were collected in static mode. In order to evaluate the effect of multipath on the position, the data files are supposed to be processed in kinematic mode, so that one position is estimated by the program for each time epoch (e.g. every 15 seconds). Therefore, the next step is to post process a kinematic baseline.

4. Before processing the data, "Store continuous as trajectory" should be set to "yes" under Project -> Project Settings -> Baseline Processing -> General. Precise orbits should be applied to get the best position accuracy by selecting "Precise" under Project -> Project Settings -> Baseline Processing -> General -> Ephemerids type.
5. The roving segment of KTH\_0 point ought to be forced to be processed as continuous data. It is done in the project explorer window, by clicking "expand Imported Files", then expanding the rover file name (0kth\*.16o), then double clicking the station name, which will open the properties window in the right side of the screen, with the "force continuous" icon (formed like a snake) in the upper right corner, clicking the icon (Figure 2.4).

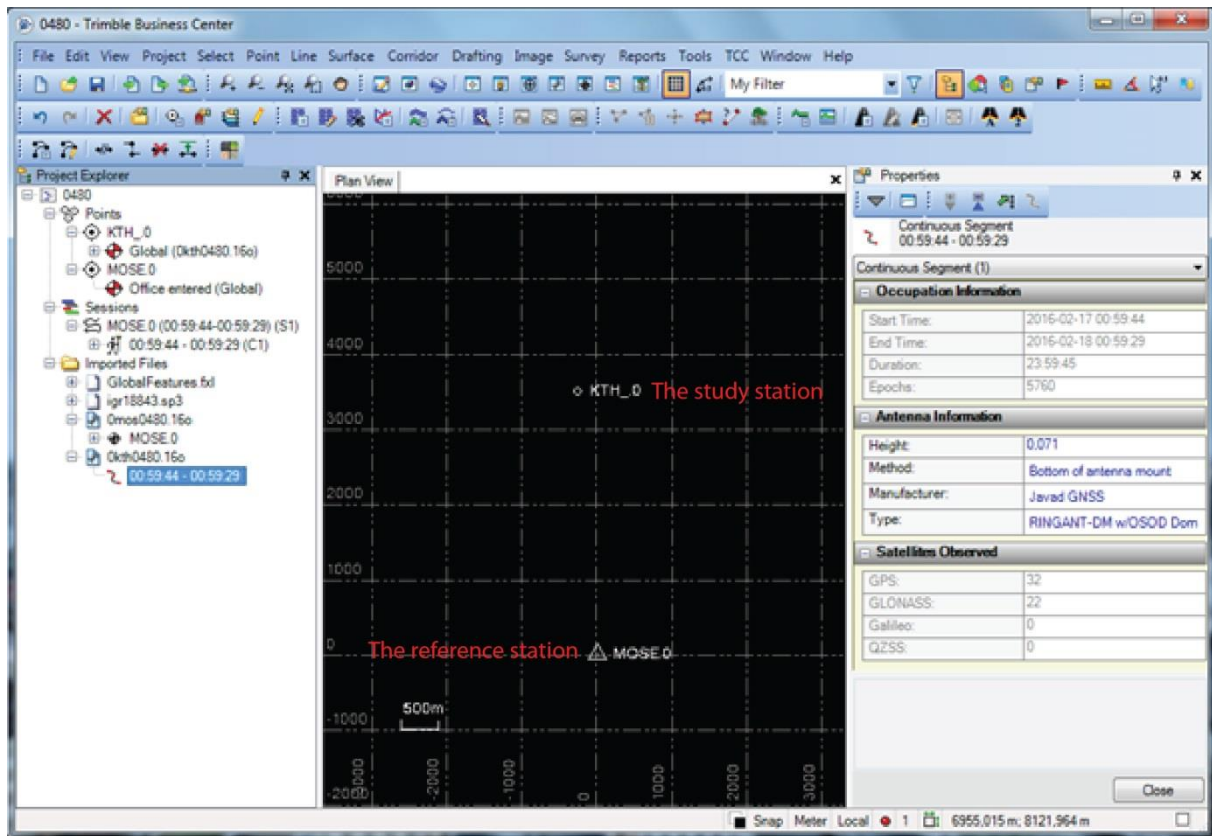


Figure 2.4 Process data in TBC.

6. The baseline between the study station and the reference station is processed using precise orbits. The baseline processing is initiated from the Project Explorer window by right clicking on the session and choosing Process Baselines. Then the results should be saved.
7. The positions are exported under File -> Export. With the Export panels open in the right side of the screen. Survey -> Trajectory (CSV) file exporter is selected. Advanced Select is clicked under Options, then Trajectory is chosen under Select and finally "all of this data type" is clicked. A suitable file name can be picked after Apply and OK being clicked. The settings ought to be double-checked and all coordinate components should be exported (latitude, longitude, height). Finally Export is clicked (Figure 2.5). The following analyses are based on the exported results.

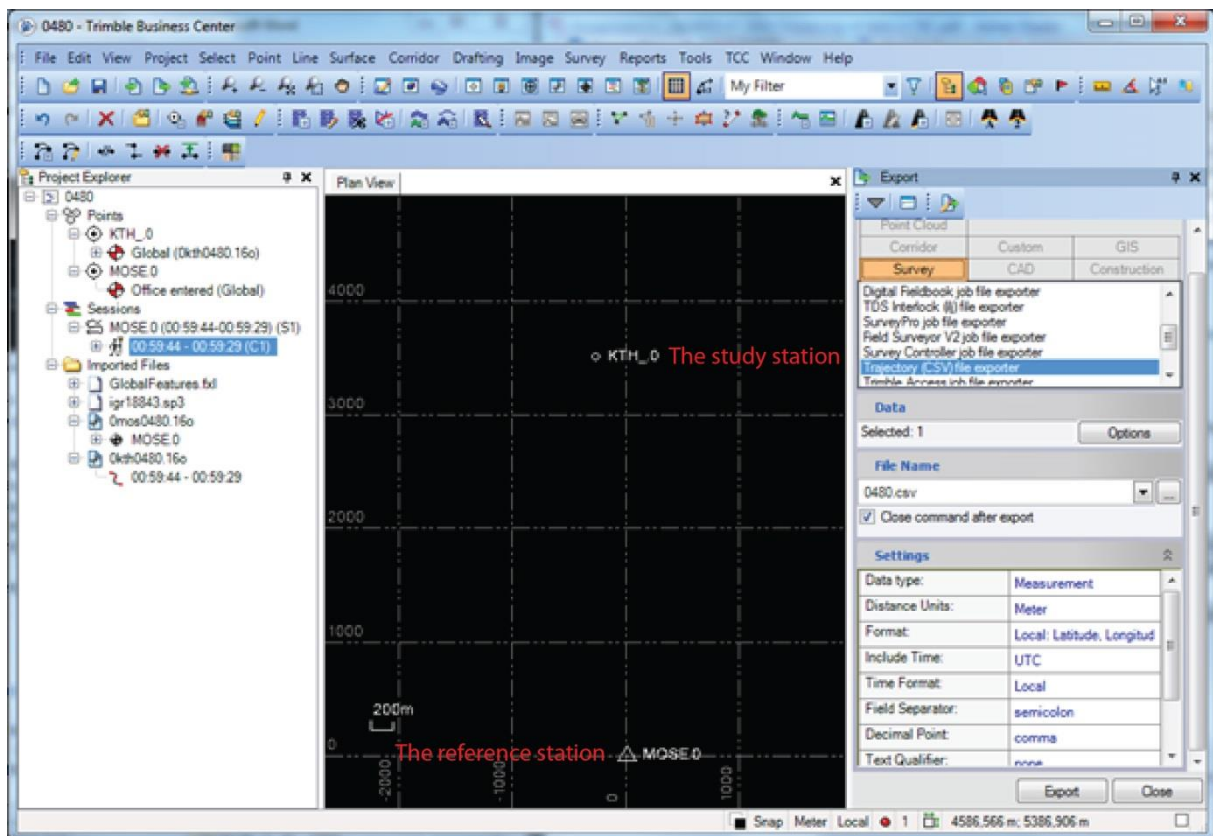


Figure 2.5 Export data from TBC.

### 2.1.2 Time series and correlation analyses

The exported .csv files contain information about latitude, longitude and height of each time interval for the study station. The following analyses will concentrate on the height value because it has a larger uncertainty than the horizontal position, so effects of multipath will be easier to detect. Its changes over time can demonstrate clearly whether or not multipath that cannot be ignored, exists in the study station.

Time series analysis is carried out on datasets of different days in MATLAB. It starts with plotting two daily variations against each other. If a common pattern is detected, datasets of more than two days can be added to the plot to reach a sound conclusion. One extra zoomed-in view for a shorter time period is provided for each figure for a better visualization effect. The four-minute-shift is taken into consideration on a daily basis, since the signals repeat themselves after 23 hours and 56 minutes.

Quantitative analysis is conducted for the purpose of drawing more convincing conclusions. To begin with, the correlation between two datasets of the same time intervals can be calculated and analysed with the consideration of the four-minute shift. Then with the purpose of investigating the correlation further, the same calculation and analysis should be done on more datasets of the same time intervals. The result will be displayed in a correlation matrix.

## 2.2 RINEX analysis

### 2.2.1 Theory description

As mentioned in the Introduction section, there is no general model of the multipath effect because of the time- and location-dependent geometric situation. The influence of the multipath, however, can be estimated by using a combination of pseudorange code and carrier phase measurements. The principle is based on the fact that the troposphere, clock errors, and relativistic effects influence code and carrier phases by the same amount. However, this is not true for ionospheric refraction and multipath, which are frequency dependent (Hofmann-Wellenhof et al., 2008). Therefore, forming corresponding differences for code ranges and carrier phases, all mentioned effects except for ionosphere and multipath are cancelled. And the residuals, apart from the noise level, reflect the multipath effect.

Multipath effect for pseudorange code observations (P1 and P2) can be demonstrated in the following equation (Hofmann-Wellenhof, 2008):

$$R_{P2} - R_{P1} = (\rho_{P2} - \rho_{P1}) + (d\rho_{P2} - d\rho_{P1}) + [c(\delta_{rP2} - \delta_{P2}^S) - c(\delta_{rP1} - \delta_{P1}^S)] + (I_{P2} - I_{P1}) + (T_{P2} - T_{P1}) + (v_{P2} - v_{P1}) \quad (1)$$

Where  $R$  is measured pseudorange in metres,  $\rho$  is geometric distance between receiver and satellite,  $d\rho$  is orbit error,  $c$  is speed of light,  $\delta_r$  and  $\delta^S$  are receiver and satellite clock error,  $I$  is signal delay in ionosphere,  $T$  is signal delay in troposphere, and  $v$  is multipath, receiver noise etc. It should be kept in mind that the satellite and receiver code and phase biases exist in the data. The influence of these is limited, and thus they are ignored during the computation. The differences in geometric distance, orbit error, clock error, and tropospheric delay can be seen as zero. The residual effect of the difference in ionospheric delay changes slowly and doesn't vary much from one epoch to another. Therefore, the majority of the remaining difference in code observations is the difference in multipath and receiver noise, where multipath is expected to be the dominant part.

Multipath effect for carrier phase observations (L1 and L2) on the other hand can be demonstrated in the following equation (Hofmann-Wellenhof et al., 2008):

$$\varphi_{L1} - \varphi_{L2} = (\rho_{L1} - \rho_{L2}) + (d\rho_{L1} - d\rho_{L2}) + [c(\delta_{rL1} - \delta_{L1}^S) - c(\delta_{rL2} - \delta_{L2}^S)] + (\lambda_{L1}N_{L1} - \lambda_{L2}N_{L2}) - (I_{L1} - I_{L2}) + (T_{L1} - T_{L2}) + (v_{L1} - v_{L2}) \quad (2)$$

Where  $\varphi$  is measured phase observation in metres,  $\lambda$  is wavelength, and  $N$  is ambiguity. The other variables are of the same meaning as the equation above. The difference in wave length multiplying ambiguity remains constant which plays as an offset. It means the difference in carrier phase observations is the difference in multipath plus an extra offset. In order to make this difference in the same scale as the difference for the code observations, scaling was applied by having it divided by  $10^5$  for the datasets used in this thesis project.

### 2.2.2 Data collection, processing and analysis

RINEX analysis has been conducted again within MATLAB and TBC. The procedure can be divided into four steps: data collection, processing in MATLAB, analyses in MATLAB assisted with TBC, and conclusion (Figure 2.6). They will be demonstrated in detail in the following paragraphs.

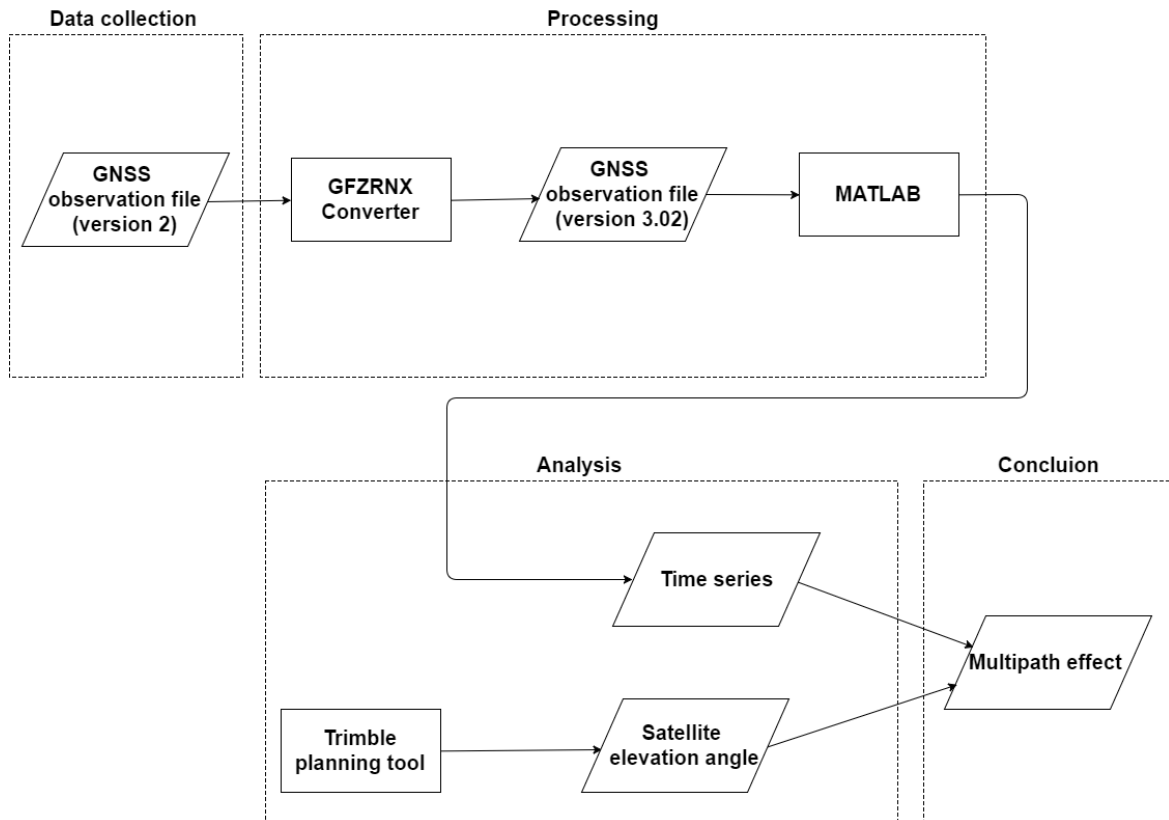


Figure 2.6 Workflow for RINEX analysis.

The data needed is mainly RINEX observation files from Lantmäteriet, which is one of the input datasets for Trimble baseline analysis. The observations of C1 and P2 are used as pseudorange code since the P1 is not logged by Lantmäteriet. The observations of L1 and L2 are used as carrier phase codes. C1 and P2 are in metres, while L1 and L2 are in cycles. Therefore, observations of L1 and L2 are multiplied by their wavelength (0.19 metre and 0.24 metre respectively). The original data is in version 2 format, and a GFZRNX converter, developed by GFZ (German Aerospace), is applied to convert the data into version 3.02. Until now, the dataset is ready for MATLAB analysis. The main function is named "readRinex302.m", whose functionality is to read RINEX files in version 3.02 and then output the observations of each time epoch for every functional satellite. Based on that, the time series figure can be plotted for an individual satellite-receiver track as the example shown in Figure 2.7.

In order to further understand the phenomenon, Trimble planning tool is applied for the calculation of satellite elevation angle and azimuth. The tool is located under Tools -> Planning. At the first place, several parameters need to be set in the Station Editor which can be found under File. The station name, approximate coordinates (latitude, longitude, and height), and the date of the data are the important parameters to be entered (Figure 2.8). It is worth noting that the elevation cut-off is set to be 10 degrees in Figure 2.8, which means that only data with elevation angle larger than 10 degrees has been analysed. Then the elevation angle for all satellites during the day can be seen by clicking Graphs -> Elevation, and the azimuth can be displayed by clicking Graphs -> Sky Plot. This kind of information is useful for the multipath analysis of different satellite-receiver track at different time of the day. As mentioned in the Introduction section, satellites at low elevation are more affected than those at high elevation. And also satellites facing the study station are also more affected by multipath noise. Therefore, a higher noise

level is expected for satellites at low elevation angles and located directly opposite to the place where the study antenna is mounted.

It is worth noting that the time in the RINEX file is GPS time which roughly corresponds to UTC time, while the time is given as UTC + 2 hours in Trimble planning tool (Figure 2.8). The two hour offset used by the Trimble software is introduced to fit local Swedish daylight savings time. Therefore, the time is shifted behind by two hours when the data from RINEX file are plotted in MATLAB, in order to make the two times comparable. It mainly results in two phenomena. Firstly, there are data displayed after 24:00 of the day and they are actually the data from midnight to 02:00 in the morning of the next day. Secondly, the data before 02:00 in the morning of the day are missing and they can be found in the data after 24:00 of the previous day (Figure 2.9).

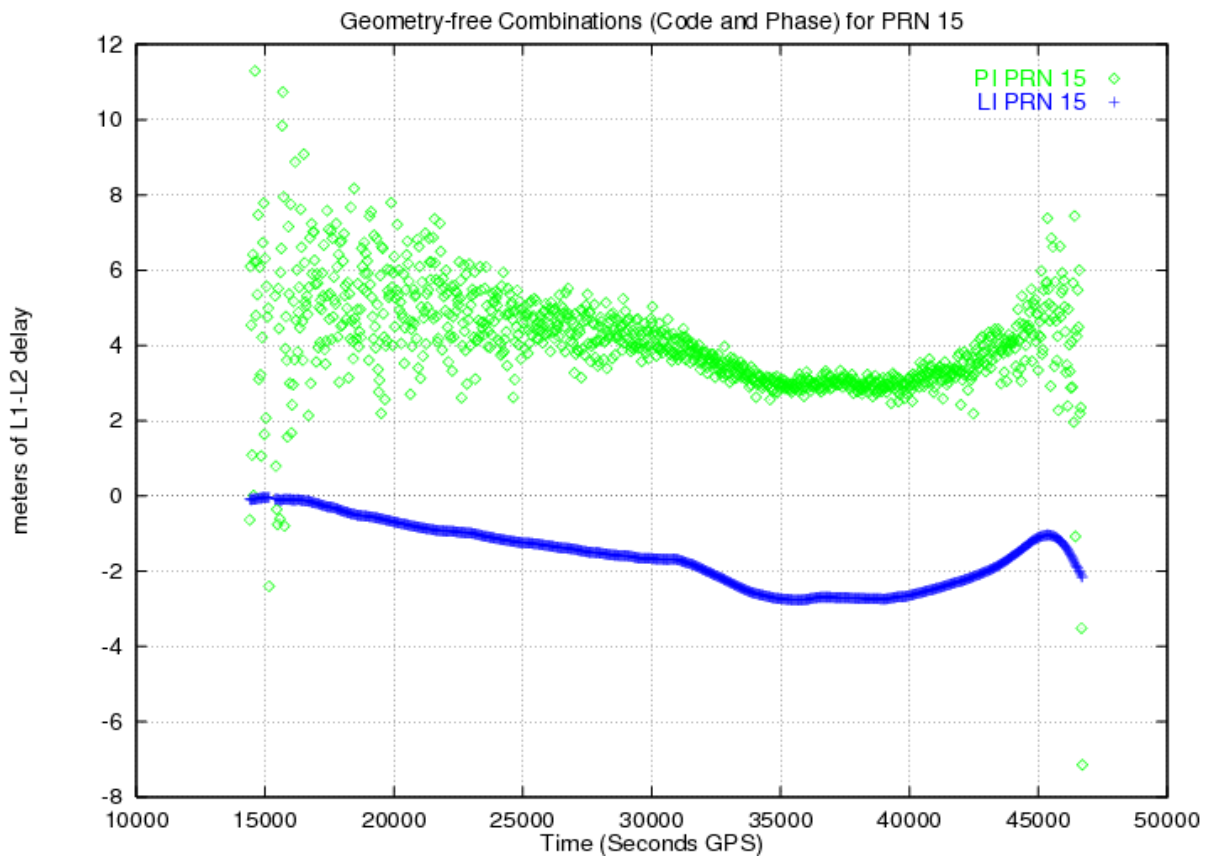


Figure 2.7 Multipath effect on GPS pseudorange and carrier phase observations (source: [http://www.navipedia.net/index.php/File:Multipath\\_Fig\\_2.png](http://www.navipedia.net/index.php/File:Multipath_Fig_2.png); data accessed: 24<sup>th</sup> Apr 2016).

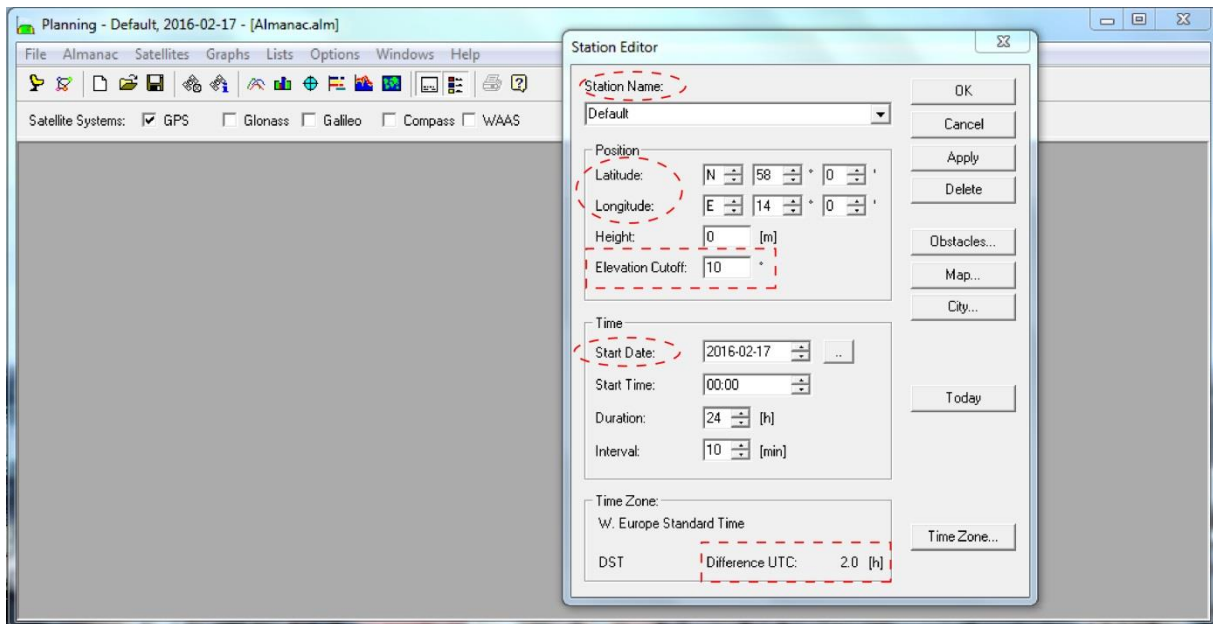


Figure 2.8 Trimble planning tool.

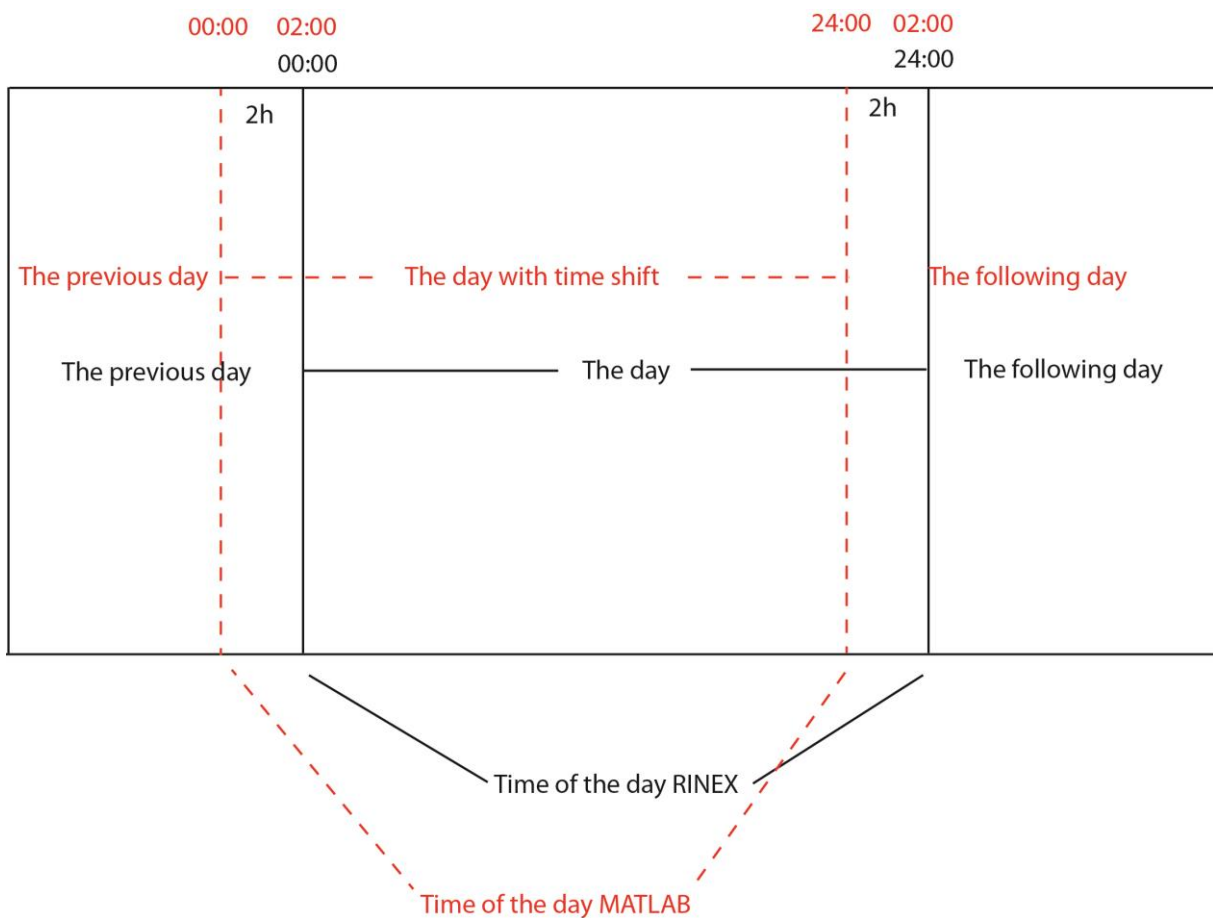


Figure 2.9 Illustration for time shift.

### 3. Experiment and application

#### 3.1 Experiment with station KTH

##### 3.1.1 Result of Trimble baseline analysis

Station KTH is selected as the experimental station, since significant multipath may exist due to the reflection of the large mirror on the upper side part of the newly-built student accommodation building close by (Figure 3.1). According to the map of SWEPOS stations from Lantmäteriet, station Mosebacke is selected as the reference station since it is the closest station to station KTH (Figure 3.2), located approximately 3.5 km away. GPS day 48 to day 57 are selected as the sample data, and they correspond to 17<sup>th</sup> February to 26<sup>th</sup> February 2016. All the ten datasets have been subject to the baseline processing analysis in the Trimble Business Center software.



Figure 3.1 Photo for the mounted antenna of station KTH.



Figure 3.2 Location of station KTH and its reference station Mosebacke (source: <https://swepos.lantmateriet.se/tjanster/kartstod/kartstod.aspx>; data accessed: 21<sup>st</sup> Mar 2016).

Firstly, data for 25<sup>th</sup> February and 26<sup>th</sup> February (GPS day 56 and 57) are plotted together (Figure 3.3) with the zoomed-in view (Figure 3.4). The values are following the similar pattern to some extent, and the pattern is more obvious in the zoomed-in view. Therefore, there is a high possibility that multipath exists in station KTH.

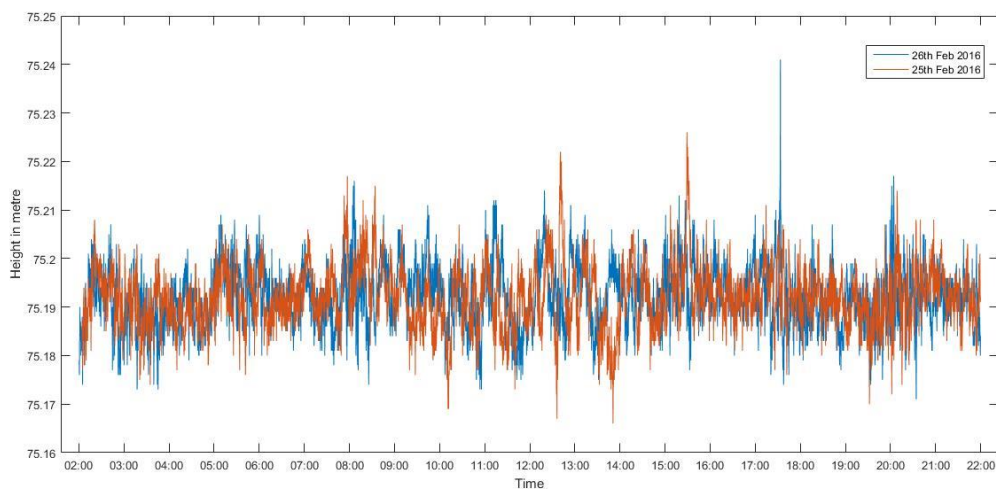


Figure 3.3 Datasets for 25<sup>th</sup> Feb and 26<sup>th</sup> Feb 2016 of station KTH.

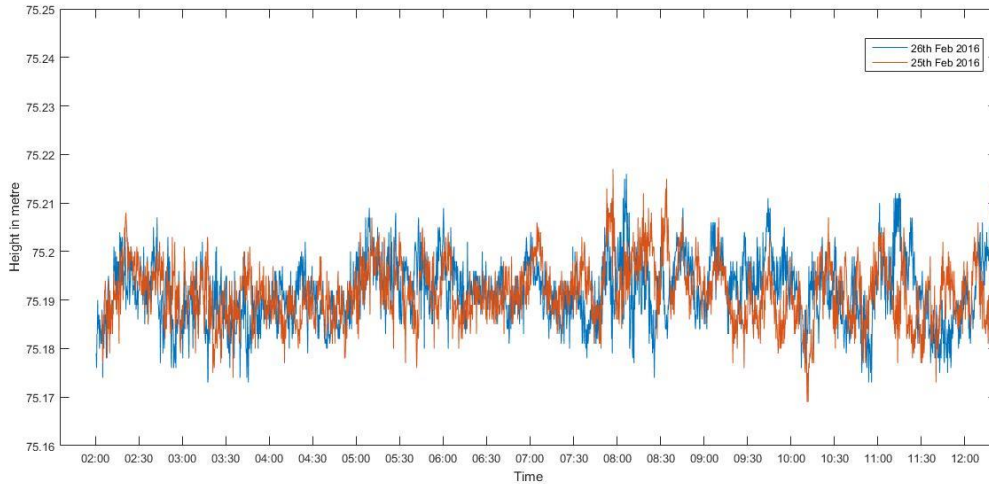


Figure 3.4 First ten-hour of Figure 3.3.

Secondly, data for ten days are plotted together (Figure 3.5) with the zoomed-in view (Figure 3.6). In Figure 3.5 values of ten days are clustered together, therefore, no clear pattern can be observed. However, in Figure 3.6 a common pattern is discernible for the 10 datasets. It is clearly observed that data for 23<sup>rd</sup> Feb (GPS day 54) with purple line have unexpected values during 16:00 and 17:00. This might be caused by human disturbances, like maintenance work on the roof of the building where the antenna is mounted, etc. And also data for 18<sup>th</sup> Feb (GPS day 49) with red line have large variations in the beginning of the day. According to the SWEPOS ionosphere monitor, there was high ionospheric activity from midnight until around six o'clock in the morning, which is probably the cause of the variations (Figure 3.7). So these two datasets are removed in order to achieve a clearer daily pattern (Figure 3.8) with the zoomed-in view (Figure 3.9).

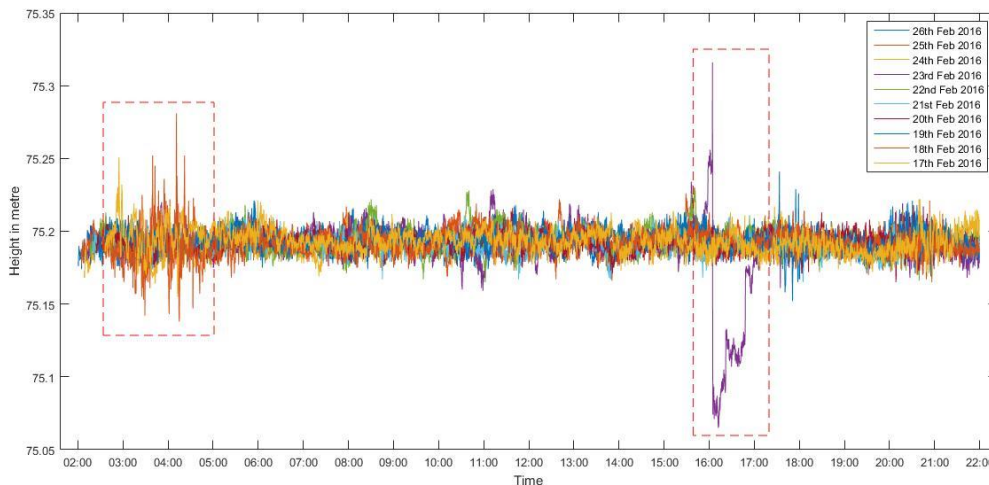


Figure 3.5 Datasets for 17<sup>th</sup> Feb to 26<sup>th</sup> Feb 2016 of station KTH.

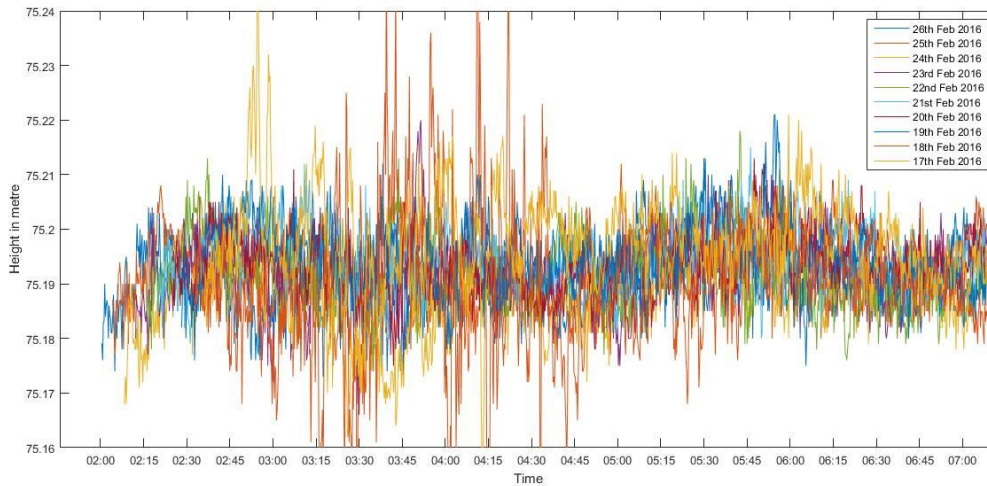


Figure 3.6 First five-hour of Figure 3.5.

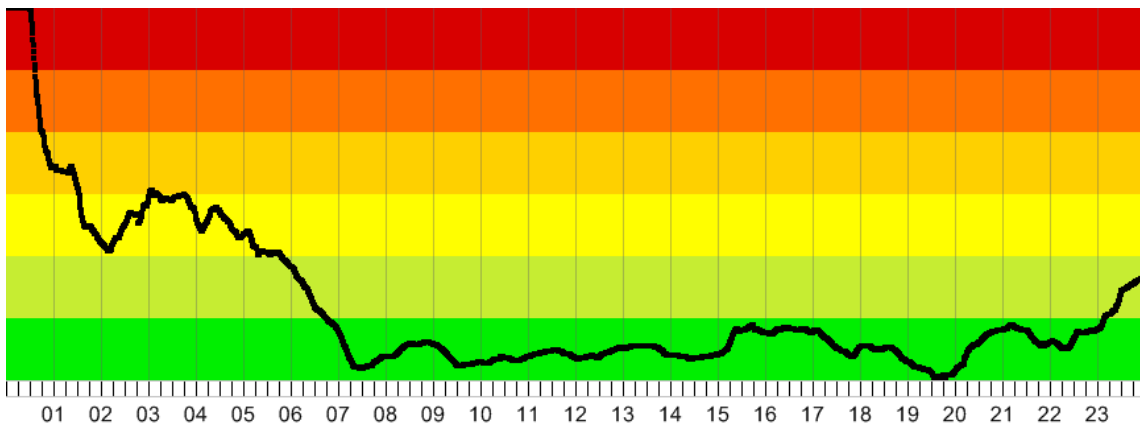


Figure 3.7 Ionospheric activity of Svealand on 18<sup>th</sup> Feb 2016 from SWEPOS ionosphere monitor (source: <https://swepos.lantmateriet.se/tjanster/jonomonitor/jonomonitor.aspx>; data accessed: 13<sup>th</sup> May 2016).

Without outliers, the common pattern is again obvious among the eight datasets which indicate a long time period in Figure 3.8 and Figure 3.9. From the time series analyses of images, it is highly possible that multipath cannot be ignored in station KTH.

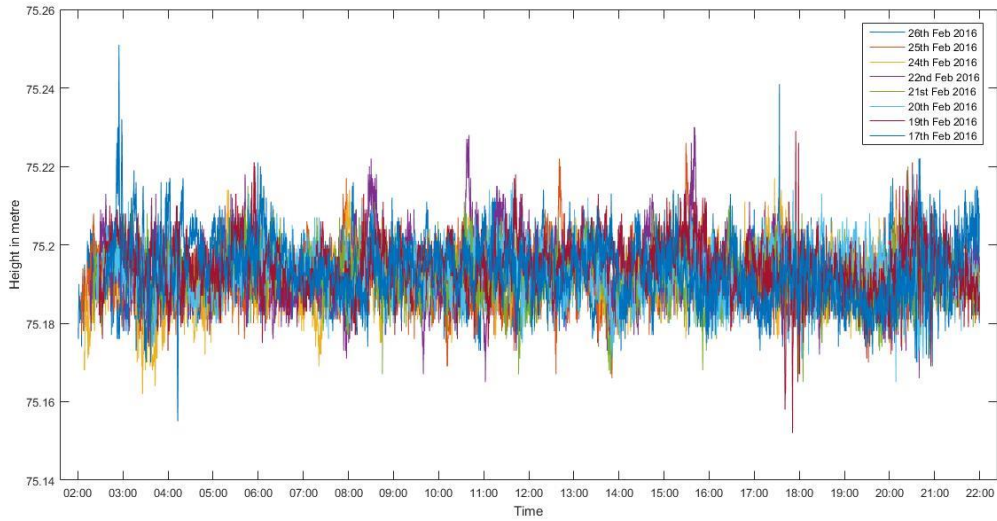


Figure 3.8 Datasets for 17<sup>th</sup> Feb to 26<sup>th</sup> Feb 2016 of station KTH, except for 18<sup>th</sup> Feb and 23<sup>rd</sup> Feb.

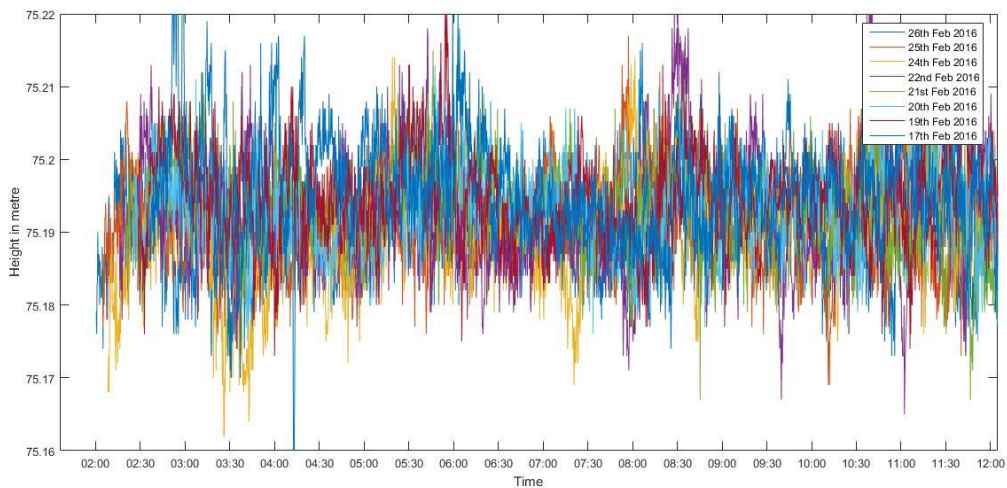


Figure 3.9 First ten-hour view of Figure 3.8.

As mentioned in the Method section, the four-minute-shift needs to be considered. It turns out that this shift is vital to the quality of results. Take 25<sup>th</sup> February and 26<sup>th</sup> February (GPS day 56 and 57) as an example, they are positively related with a correlation as 0.0728 if the algorithm is conducted directly on the datasets. However, the correlation changes to 0.3511 if the four-minute-shift is taken into consideration (Figure 3.10).

```

>> corrccoef(H_0560, H_0570)

ans =

    1.0000    0.0728
    0.0728    1.0000

>> corrccoef(H_0560(17:4799), H_0570(1:4783))

ans =

    1.0000    0.3511
    0.3511    1.0000

```

Figure 3.10 Correlation between two datasets.

In order to investigate the correlation more deeply, the correlation is conducted on all the ten days' datasets on the basis of the four-minute-shift. The first thing to consider is to make all the datasets comparable by ensuring they are of the same length and thus have the same time intervals. By checking the data, all the datasets have 4799 records, except for datasets of GPS day 50 and 55 with 4798 records. Two missing records are found by comparing the two datasets with one standard dataset respectively (Figure 3.11), and then the records with these two times are deleted from all datasets. Therefore, all the ten datasets have 4797 records for the same time intervals, and now they are ready for correlation calculation.

```

>> setdiff(T_0560, T_0550)

ans =

    17:36:44

>> setdiff(T_0560, T_0500)

ans =

    08:59:59

```

Figure 3.11 Missing records for GPS day 55 and 50.

The result of a correlation matrix is displayed in Table 3.1. Overall the ten datasets are positively correlated to each other with the highest correlation as 0.3824. It is safe to draw conclusion that multipath does exist in station KTH which has a significant influence on the GNSS signals. It can also be seen from the table that low correlation values smaller than 0.1000 only appear in GPS day 54 and day 49, which corresponds to the days with outliers as identified in the previous section.

Table 3.1 Correlation matrix for the 10 datasets of station KTH

	48	49	50	51	52	53	54	55	56	57
48	1									
49	0.1274	1								
50	0.2788	0.1840	1							
51	0.1767	0.1675	0.3050	1						
52	0.3042	0.1834	0.3064	0.3824	1					
53	0.1917	0.2047	0.2975	0.3289	0.3100	1				
54	0.1285	0.0779	0.2138	0.2274	0.0861	0.1738	1			
55	0.1245	0.1652	0.2453	0.2982	0.2903	0.3224	0.0646	1		
56	0.1253	0.1162	0.2321	0.2798	0.3223	0.3527	0.1362	0.3824	1	
57	0.2013	0.1780	0.2879	0.2521	0.3271	0.2659	0.0583	0.3530	0.3491	1

### 3.1.2 Result of RINEX analysis

Data of 26<sup>th</sup> February, 2016 (GPS Calendar: Day 57) for station KTH is selected for this method. There are in total 32 GPS satellites that have observations for this station on this day. The observation for each epoch mainly includes C/A code C1, P code P2, L1 phase carrier code with its corresponding SNR value, and L2 phase carrier code with its corresponding SNR value. The newly-built student accommodation building is located in the south-west of the antenna of KTH station, and thus satellites located in the north-east of the antenna are supposed to be more affected by multipath. As mentioned in the Introduction section, satellites at low elevation angle are more influenced by multipath. Based on these two criteria, five GPS satellites – G05, G06, G15, G26, and G31, which are expected to experience more obvious multipath effect during specific time periods of the day, were selected to conduct the RINEX analysis with the help of the Planning tool of TBC. The results are displayed in the following ten figures (Figure 3.12 to Figure 3.21).

Satellite G05 has data during three time periods (00:00 – 02:00, 11:00 – 16:00, and 22:00 – 24:00) according to the Planning tool (Figure 3.12). However, in MATLAB plot the data for 00:00 – 02:00 of this day is missing and there are data for 00:00 – 02:00 of the following day, which is caused by the two-hour time shift as explained in the previous section. Besides this, there are several typical phenomena to be explained in Figure 3.13. First of all, the multipath effect does exist, which can be clearly seen from the variations of difference in pseudorange code over time. The multipath effect for carrier phase code (1-5cm) is hard to be observed since the scale of the y-axis is in metres. Secondly, the largest noise exists in the edges, and it is due to the low elevation rays at the rising and setting of the satellite. Thirdly, the range of the variation for pseudorange code of time period 22:00 – 24:00 is larger than that of time period 12:00 – 15:00. This may be caused by two reasons: according to Elevation plot of the Planning tool, the elevation angle is below 30 degree for 22:00 – 24:00, while it is varying from 30 degree to 60 degree for 12:00 – 15:00; and with reference to the Sky plot, the satellite is located in the north-east of the antenna with the azimuth ranging from 0 to 90 degree for the time period 22:00 – 24:00, while it is in the opposite position for the other period. Therefore, it is proved that multipath has a stronger influence on satellites at lower elevation angle and with specific azimuth related to the antenna and its surrounding environment.

For the other selected satellites - G06, G15, G26, and G31, the observed patterns are rather analogous. Satellite G06 has data for two time periods – 08:00 – 12:00 and 19:00 – 22:00. The period 19:00 – 22:00 when G06 is at low elevation angle and with azimuth smaller than 90 degree experiences larger multipath effect compared to 08:00 – 12:00 when the elevation angle is much higher and the azimuth is over 180 degree (Figure 3.14 and Figure 3.15). Satellite G15 also has observations for two time periods – 02:00 - 04:00 and 15:00 – 19:00 (Figure 3.16). It is even more obvious that the variation for pseudorange of 02:00 – 04:00 is much larger than that of 15:00 – 19:00 (Figure 3.17). The satellite is at two opposite positions during the two periods as displayed in Figure 3.16, and the difference in elevation angles is even larger for these two periods. Satellite 26 has data for three time periods – 00:00 – 03:00, 10:00 – 12:00, and 22:00 – 24:00 (Figure 3.18). However, the data for 00:00 – 02:00 is missing in the MATLAB plot because of time shift (Figure 3.19). The variation of difference in pseudorange codes is rather large for 10:00 – 12:00 as expected, while the variations are relatively small for the other two time periods. They correspond to the elevation angles and the azimuths displayed in Figure 3.18. Finally for satellite 31, Figure 3.20 shows that there are data for three time periods – 00:00 – 01:00, 07:00 – 10:00, and 21:00 – 24:00 (Figure 3.20). Again, the data before 02:00 of the day are missing in the MATLAB plot. The variation of pseudorange code observations for 07:00 – 10:00 is still larger than that for 21:00 – 24:00 because of elevation angle and azimuth differences (Figure 3.21).

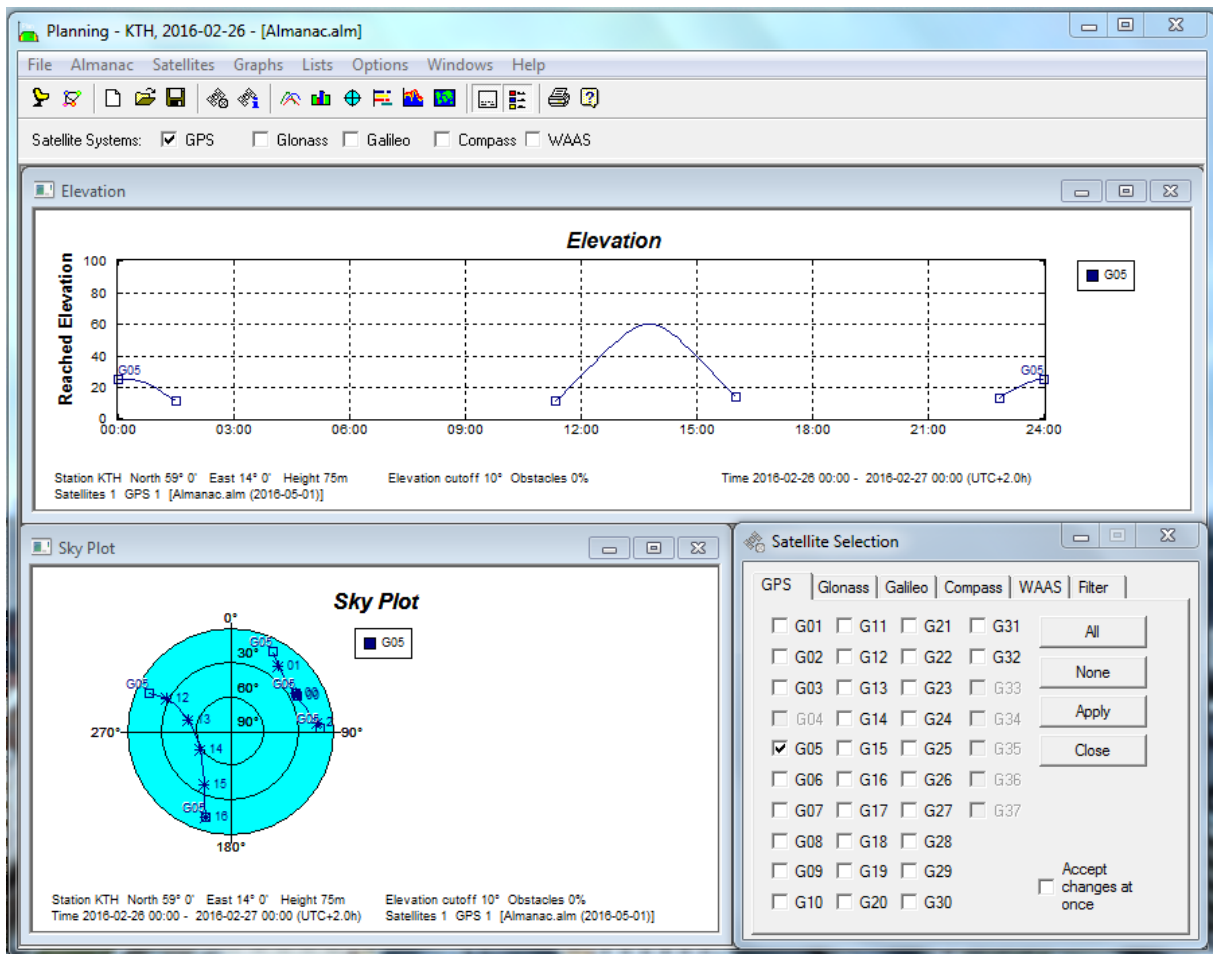


Figure 3.12 Elevation angle and azimuth of satellite G05 for station KTH on 26<sup>th</sup> Feb 2016.

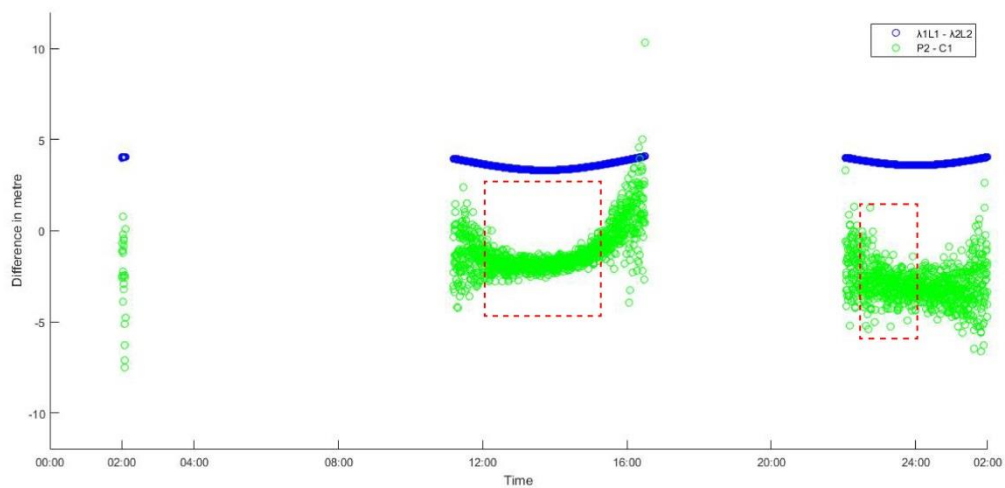


Figure 3.13 Multipath effect on pseudorange and carrier phase observations of satellite for station KTH G05 on 26<sup>th</sup> Feb 2016.

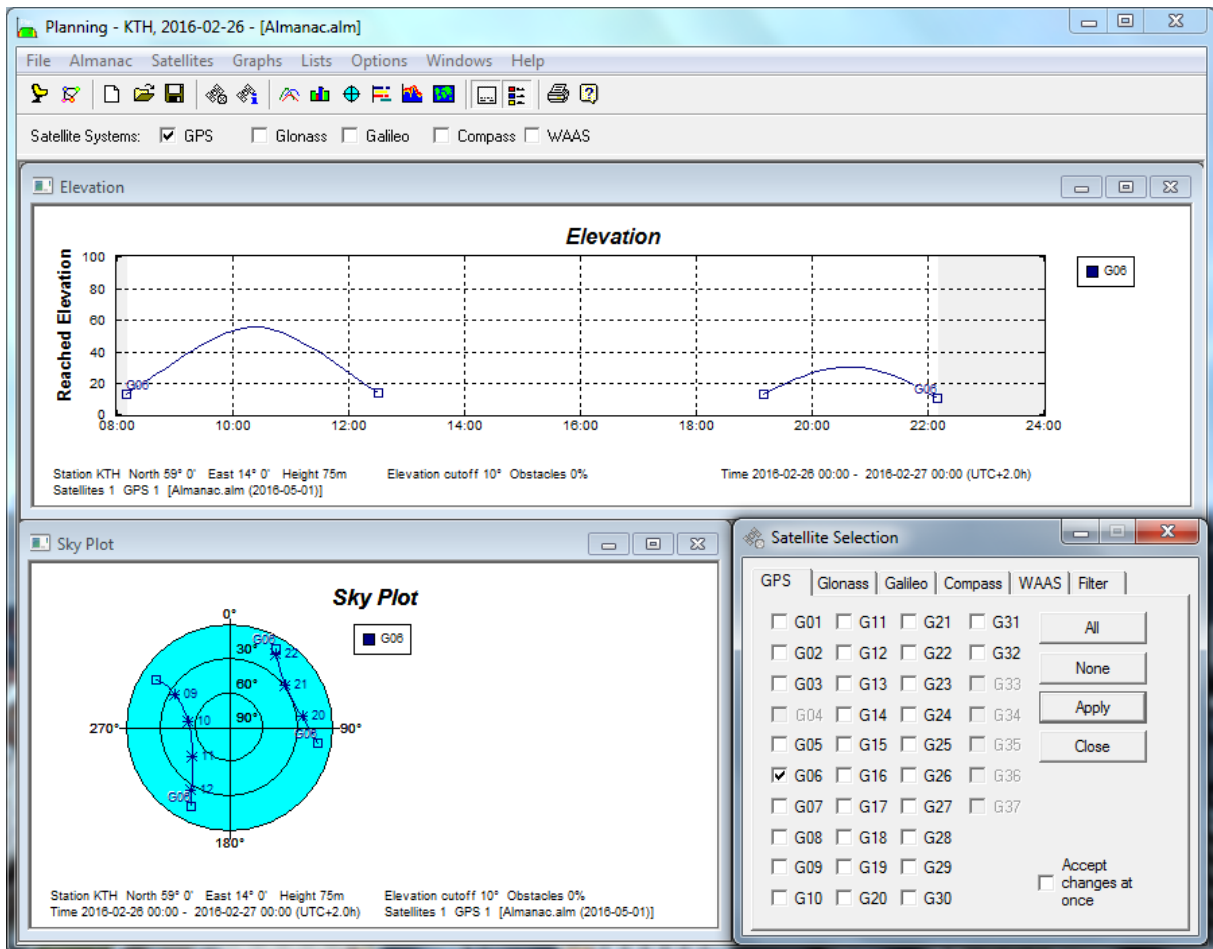


Figure 3.14 Elevation angle and azimuth of satellite G06 for station KTH on 26<sup>th</sup> Feb.

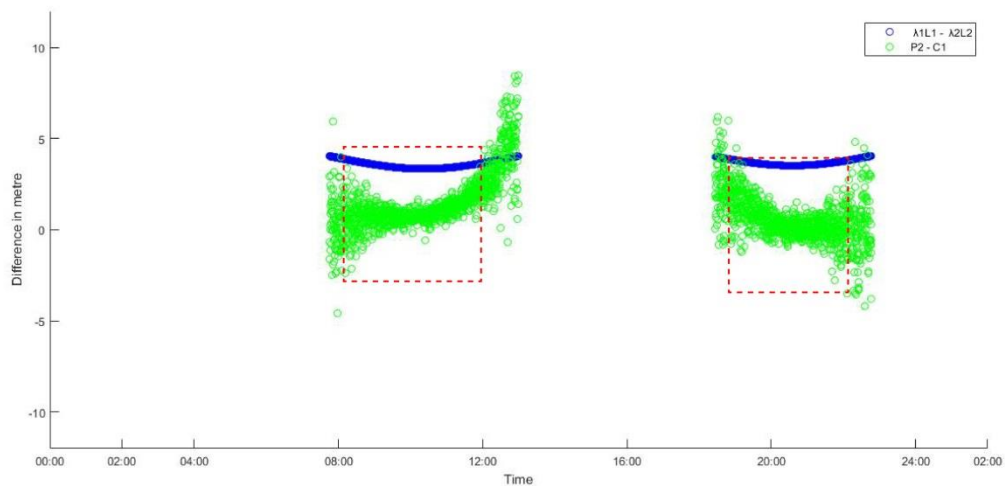


Figure 3.15 Multipath effect on pseudorange and carrier phase observations of satellite G06 for station KTH on 26<sup>th</sup> Feb 2016.

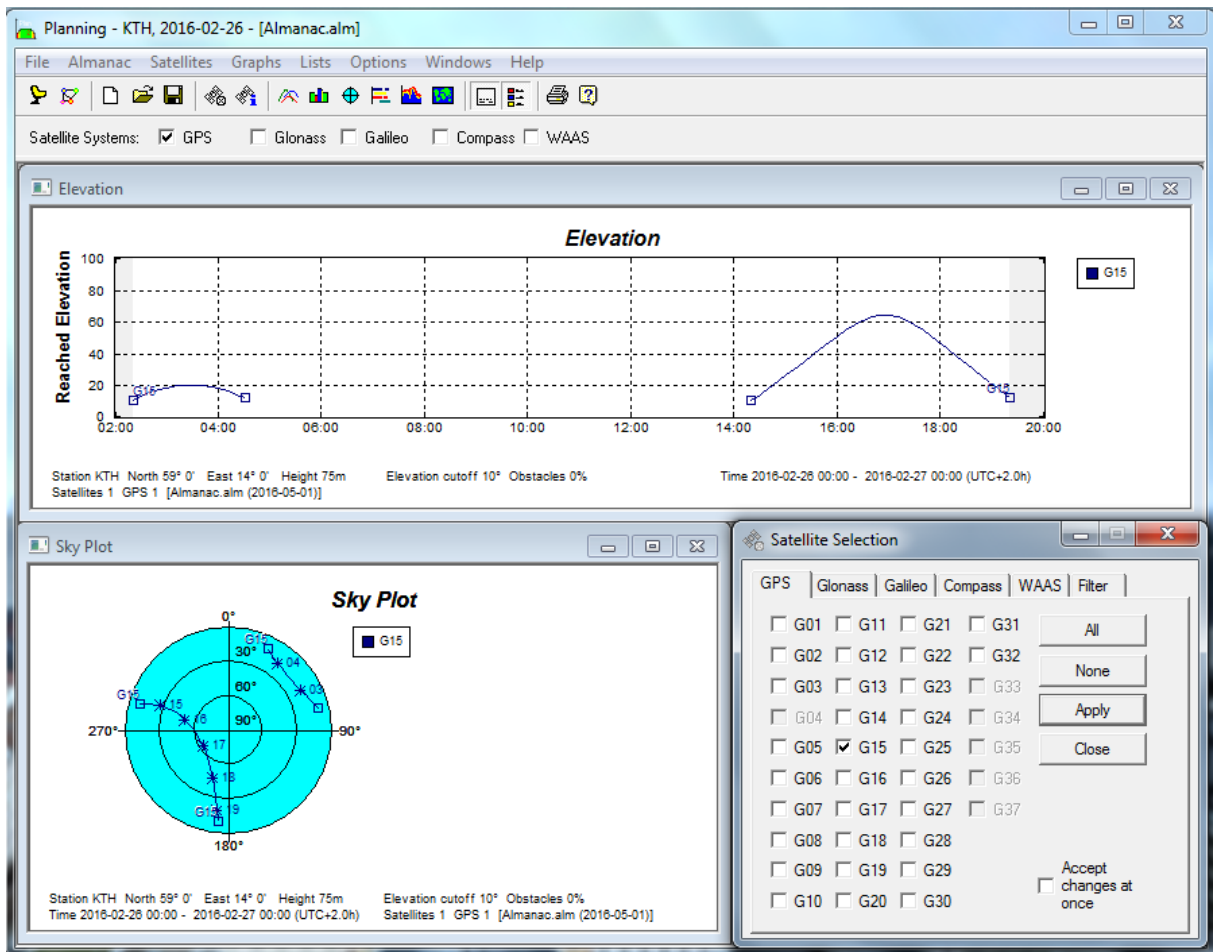


Figure 3.16 Elevation angle and azimuth of satellite G15 for station KTH on 26<sup>th</sup> Feb.

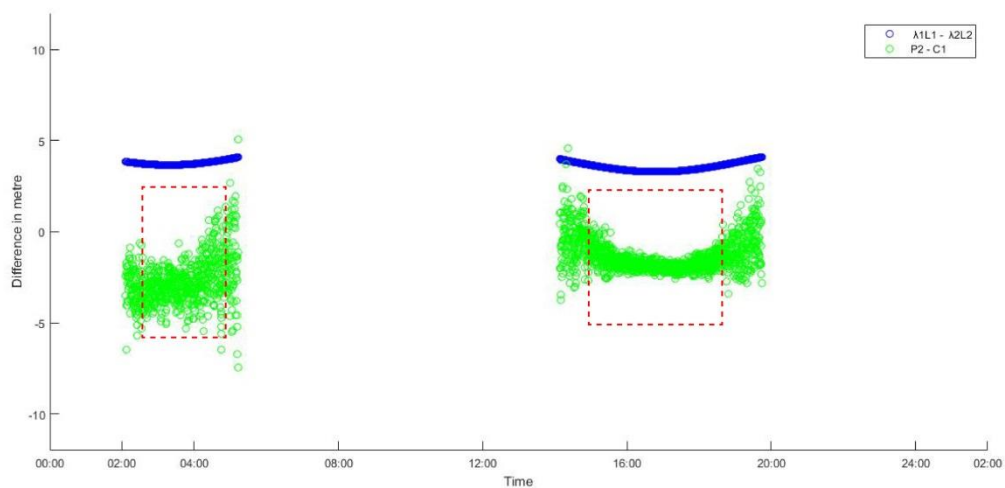


Figure 3.17 Multipath effect on pseudorange and carrier phase observations of satellite G15 for station KTH on 26<sup>th</sup> Feb 2016.

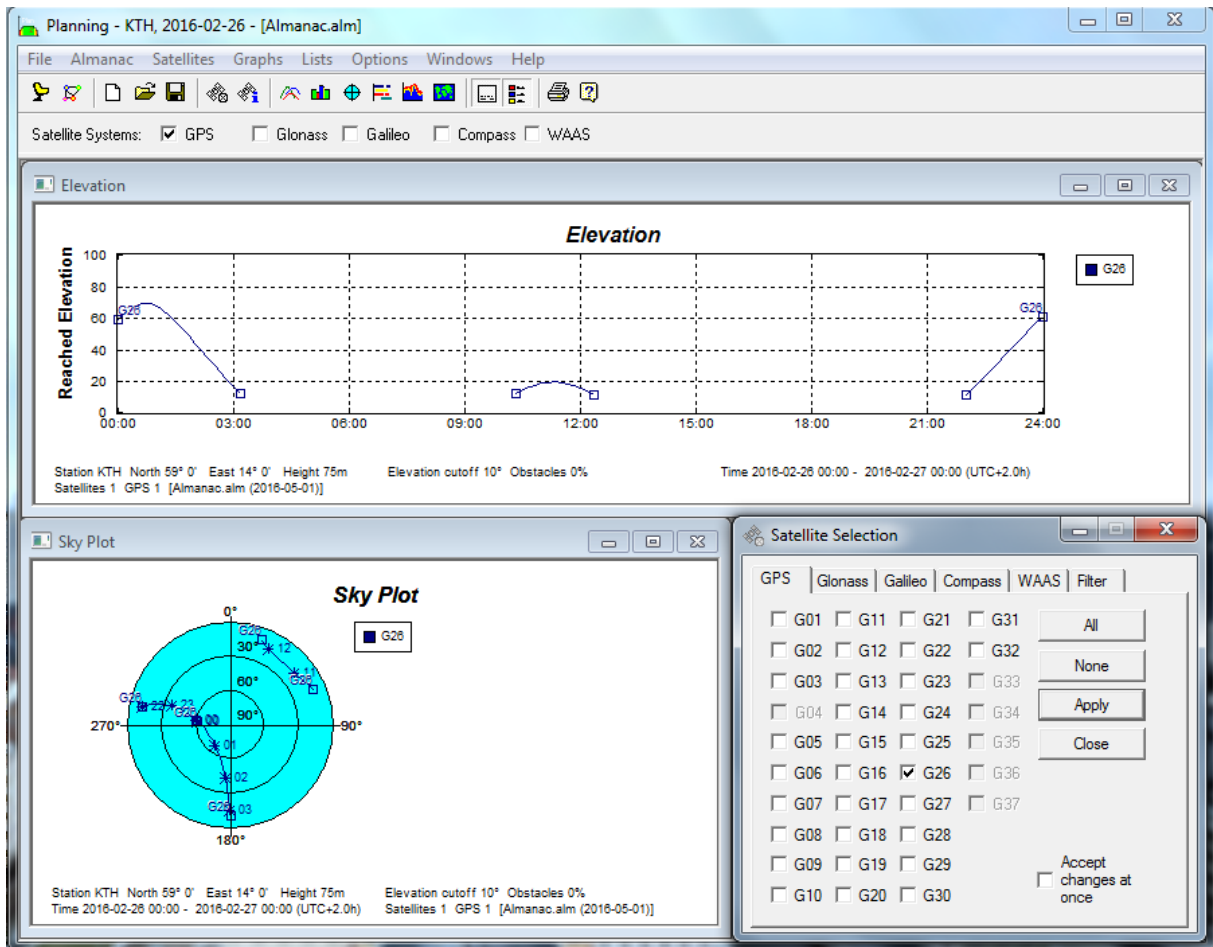


Figure 3.18 Elevation angle and azimuth of satellite G26 for station KTH on 26<sup>th</sup> Feb.

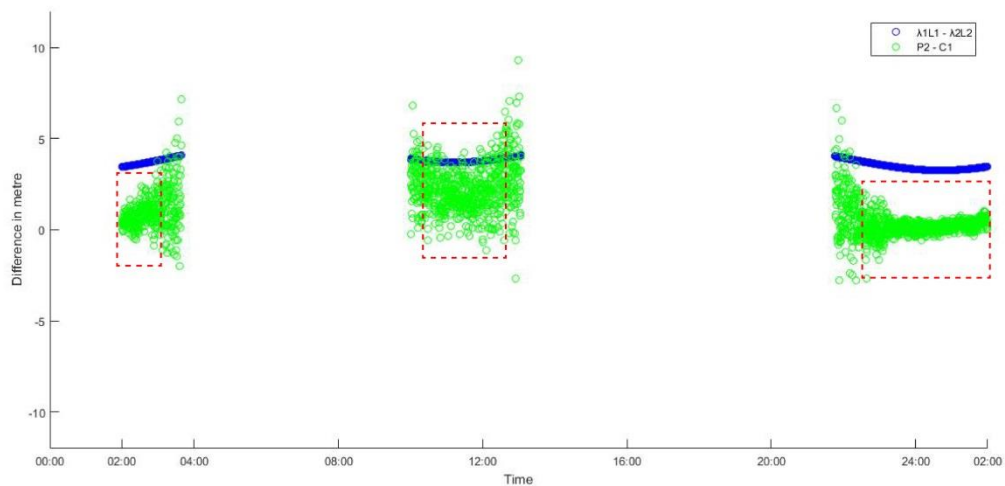


Figure 3.19 Multipath effect on pseudorange and carrier phase observations of satellite G26 for station KTH on 26<sup>th</sup> Feb 2016.

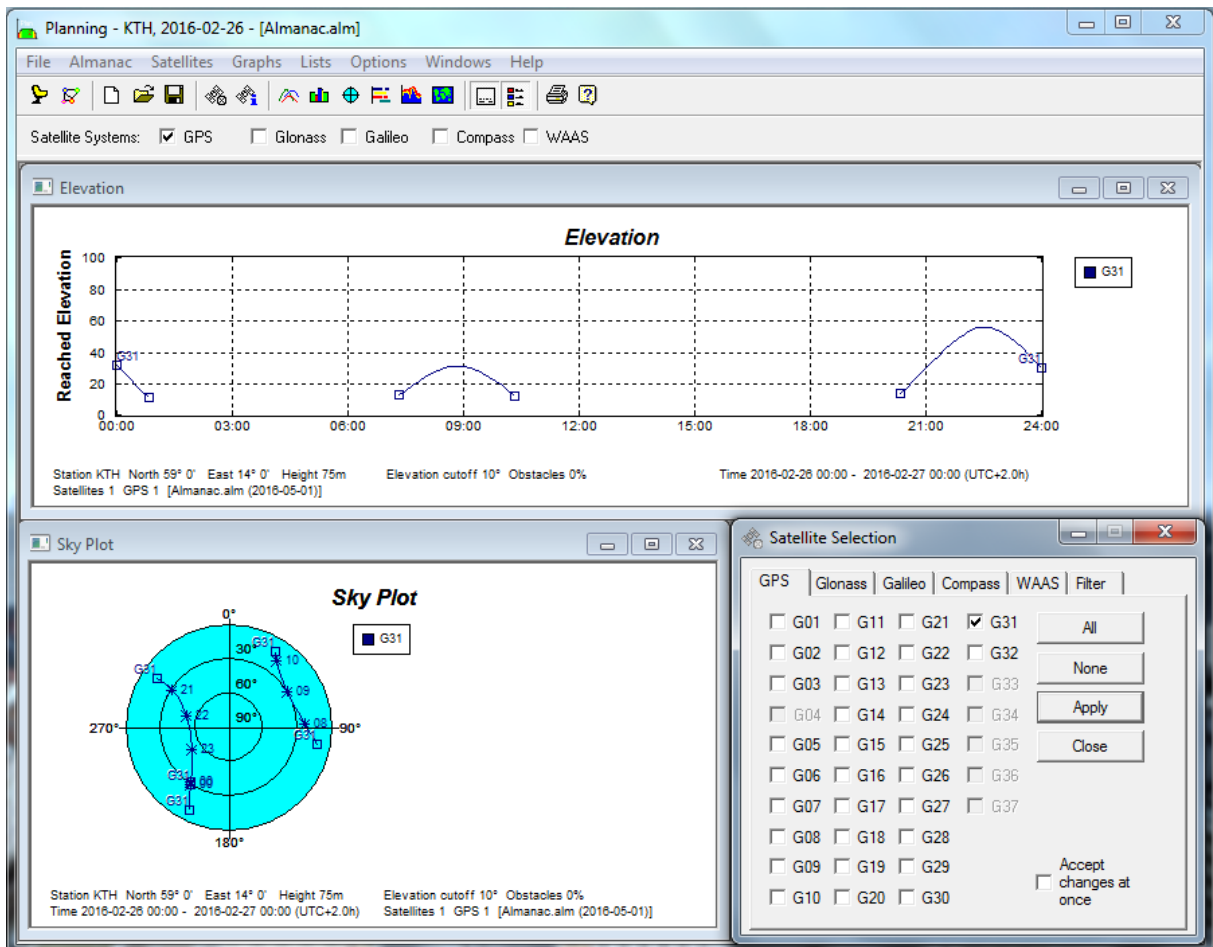


Figure 3.20 Elevation angle and azimuth of satellite G31 for station KTH on 26<sup>th</sup> Feb.

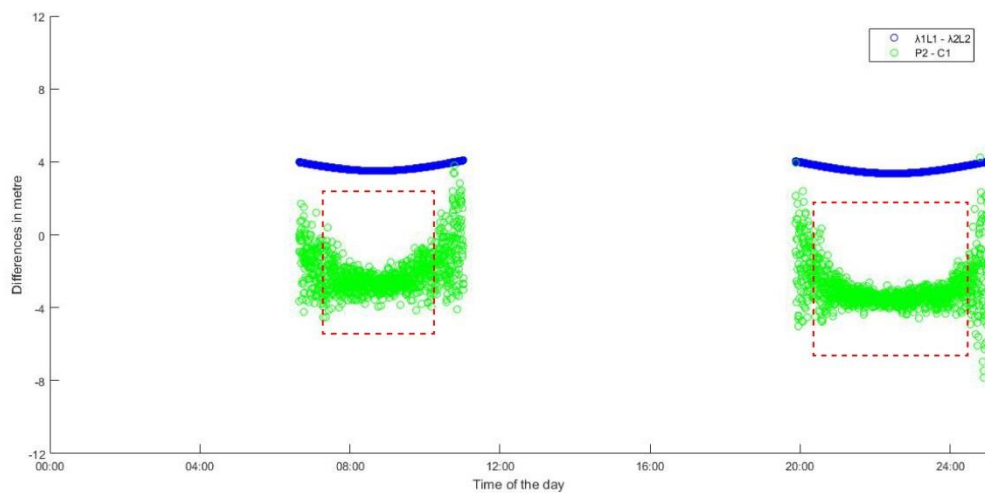


Figure 3.21 Multipath effect on pseudorange and carrier phase observations of satellite G31 for station KTH on 26<sup>th</sup> Feb 2016.

## 3.2 Application with station Vidsele and station Botsmark

### 3.2.1 Result of Trimble baseline analysis

Lantmäteriet is interested in knowing whether two other stations - Vidsele and Botsmark may be affected by multipath. Both stations are located in the Northern part of Sweden – Vidsele is close to Luleå and Botsmark is close to Umeå. The antennae are mounted on, or close to, chimneys covered with metal which could be very reflective (Figure 3.22 and Figure 3.23). For station Vidsele, the tall trees in the surrounding area may also be a causation of multipath errors. Therefore, it would be interesting to see if there perhaps is a strong multipath signal in the data from these two stations. The stations selected as the reference stations are Kåbdalis for Vidsele and Vindeln for Botsmark (Figure 3.24 and Figure 3.25).



Figure 3.22 The surrounding environment of station Vidsele, and the antenna is mounted on the side of the chimney (The photo is provided by Lantmäteriet).



Figure 3.23 Photo for the mounted antenna of station Botsmark (The photo is provided by Lantmäteriet).



Figure 3.24 Location of station Vidsele and its reference station Kåbdalis (source: <https://swepos.lantmateriet.se/tjanster/kartstod/kartstod.aspx>; data accessed: 2<sup>nd</sup> May 2016).

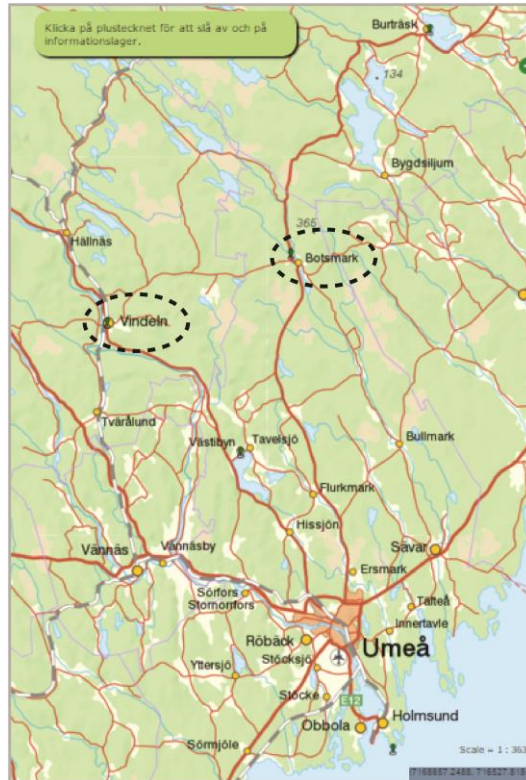


Figure 3.25 Location of station Botsmark and its reference station Vindelö (source: <https://swepos.lantmateriet.se/tjanster/kartstod/kartstod.aspx>; data accessed: 2<sup>nd</sup> May 2016).

The time period of GPS day 81 to day 85 is selected to be examined. According to the GPS calendar, they correspond to 21<sup>st</sup> March to 25<sup>th</sup> March, 2016. With the application of method one described before, the time series analysis for Vidsel and Kåbdalis is displayed in Figure 3.26 with zoomed-in view in Figure 3.27, and the correlation matrix considering the four-minute offset is shown in Table 3.2.

The datasets follow an obvious similar pattern over time as shown in Figure 3.26, with a more obvious trend displayed in Figure 3.27. As it can be seen from Table 3.2, the positive correlation is strong between datasets with highest value as 0.5946 and lowest value as 0.3233. Therefore, the conclusion can be reached safely that the surrounding environment has a significant effect on the signals of station Vidsel and causes multipath.

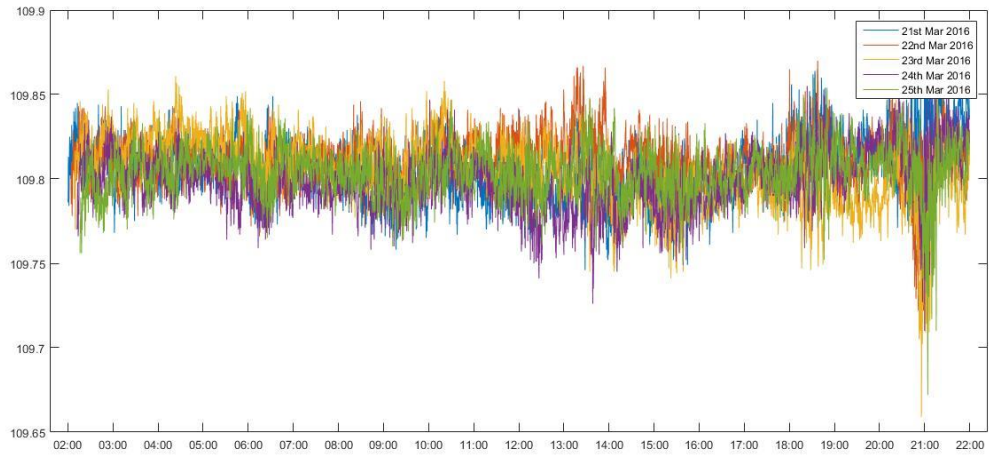


Figure 3.26 Datasets for 21<sup>st</sup> Mar to 25<sup>th</sup> Mar 2016 of station Vidsel.

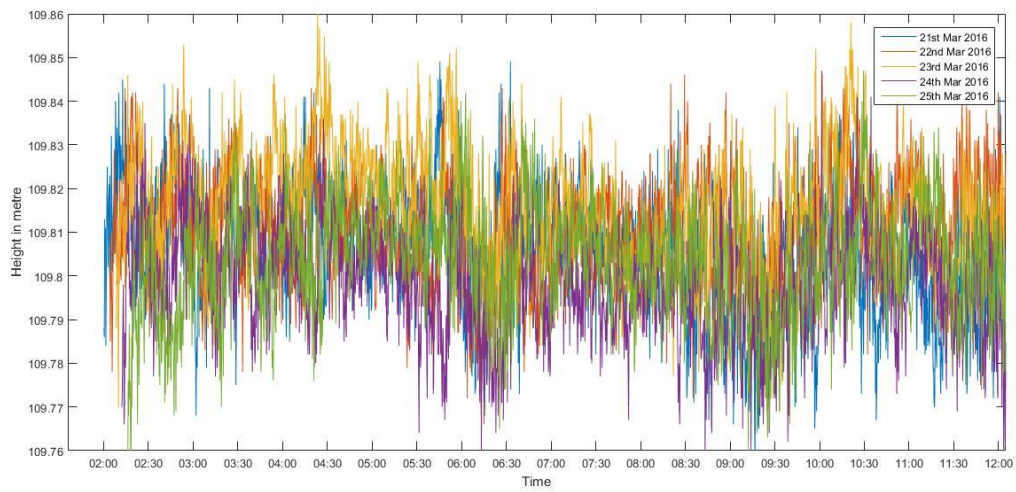


Figure 3.27 First ten-hour of Figure 3.26.

Table 3.2 Correlation matrix for the 5 datasets of station Botsmark

	81	82	83	84	85
81	1				
82	0.5946	1			
83	0.4552	0.3909	1		
84	0.4515	0.3680	0.4941	1	
85	0.3911	0.5758	0.3233	0.4501	1

The time series analysis is also conducted on station Botsmark and its reference station Vindeln. The result is shown in Figure 3.28 with its zoomed-in view in Figure 3.29. There is still a common pattern however with large variations during several time intervals (04:00-05:00 and 11:00-13.30). The phenomenon can be better demonstrated in Figure 3.29. When correlation analysis is conducted, there are large data gaps among datasets of different days. Another station Tavelsjö is also tested as the reference station for the study station. However, the same phenomenon of large data gaps is still observed. Due to the data gaps, it doesn't make much sense to perform the correlation analysis. Therefore, the influence of the reflective chimney still exists but with much noise.

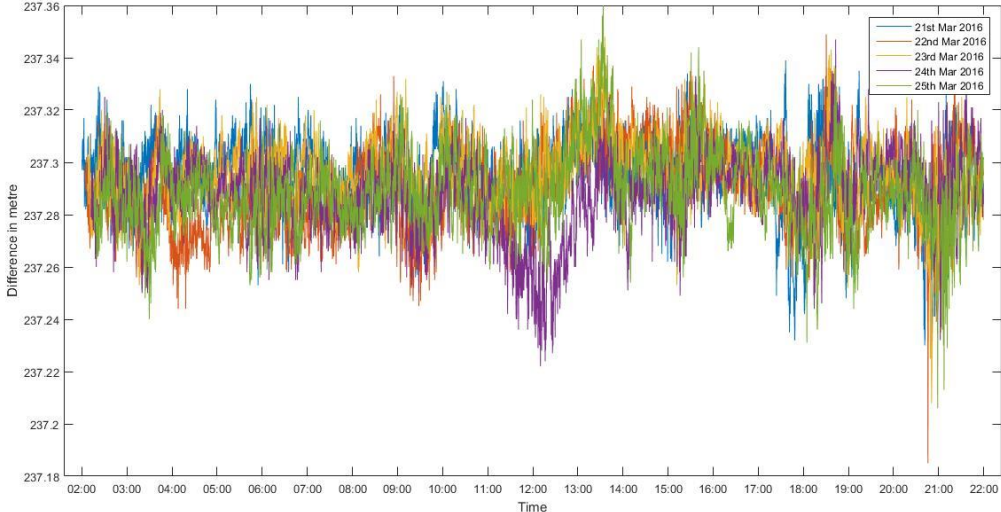


Figure 3.28 Datasets for 21<sup>st</sup> Mar to 25<sup>th</sup> Mar 2016 of station Botsmark.

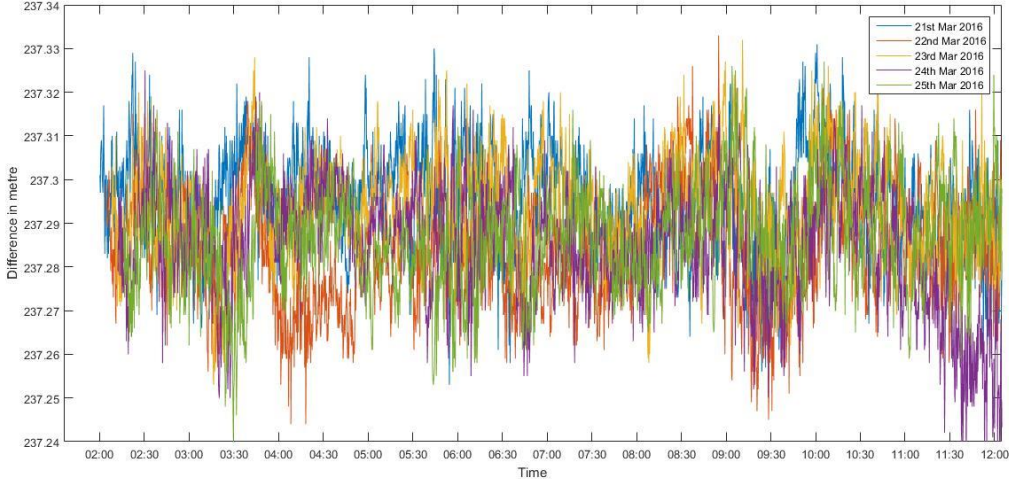


Figure 3.29 First ten-hour of Figure 3.28.

### 3.2.2 Result of RINEX analysis

Data of 25<sup>th</sup> March, 2016 (GPS Calendar: Day 85) for both station Vidsel and station Botsmark is selected for this method. The total number of GPS satellites is 32 for each station, and the observations each epoch are the same as described for station KTH. The relative location of the antenna to the reflective material in the surrounding environment is unknown for both two stations, and thus satellites which have observations covering nearly all directions should be selected. As mentioned in the Introduction section, satellites at low elevation angle are more influenced by multipath. Based on these two criteria, four GPS satellites – G03, G08, G17 and G28, which have different coverages of azimuth and are expected to experience more obvious multipath effect during specific time periods of the day, were selected to conduct the RINEX analysis with the help of the Planning tool of TBC for each station.

The results are displayed in the following 16 figures (Figure 3.30 to Figure 3.45). Analogous phenomena can be observed for these two stations as for station KTH. It is obviously indicated from the variation of difference in pseudorange code over time that multipath effect exists in both stations.

The first 8 figures (Figure 3.30 – Figure 3.37) illustrate the results for station Vidsel. From the Trimble planning tool, satellite G03 has coverage of north and south (Figure 3.30), G08 has coverage of north-east and south-west (Figure 3.32), G17 has coverage of east and west (Figure 3.34), and G28 has coverage for north-west and south-east (Figure 3.36). For satellite G03, G08, and G28, they experienced higher level of multipath noise during time periods when satellites were at lower elevation angle, which are 17:30 – 19:30 for G03, 12:00 – 15:00 for G08, and 02:00 -05:00 for G28 (Figure 3.31, Figure 3.33, and Figure 3.37). For satellite G17 however, the two time periods – 04:00 – 08:00 and 14:00 – 18:00, have elevation angle close to each other varying from 20 degree to 40 degree, which results in similar range of variation of difference in pseudorange code (Figure 3.35).

The next eight figures (Figure 3.38 – Figure 3.45) display the results for station Botsmark. Since these two stations have similar latitude and longitude, the coverages of these four satellites are briefly the same as shown in Figure 3.38, Figure 3.40, Figure 3.42, and Figure 3.44. And also the general pattern displayed in MATLAB plots is also rather similar to that for station Vidsel, as shown in Figure 3.39, Figure 3.41, Figure 3.43, and Figure 3.45. An interesting phenomenon is discernible when comparing the MATLAB plots of the same satellite for the two stations (Figure 3.31 with Figure 3.39, Figure 3.33 with Figure 3.41, Figure 3.35 with Figure 3.43, and Figure 3.37 with Figure 3.45). Plots for station Vidsel tend to have more noise in the difference in pseudorange codes than those for station Botsmark, which can be investigated further.

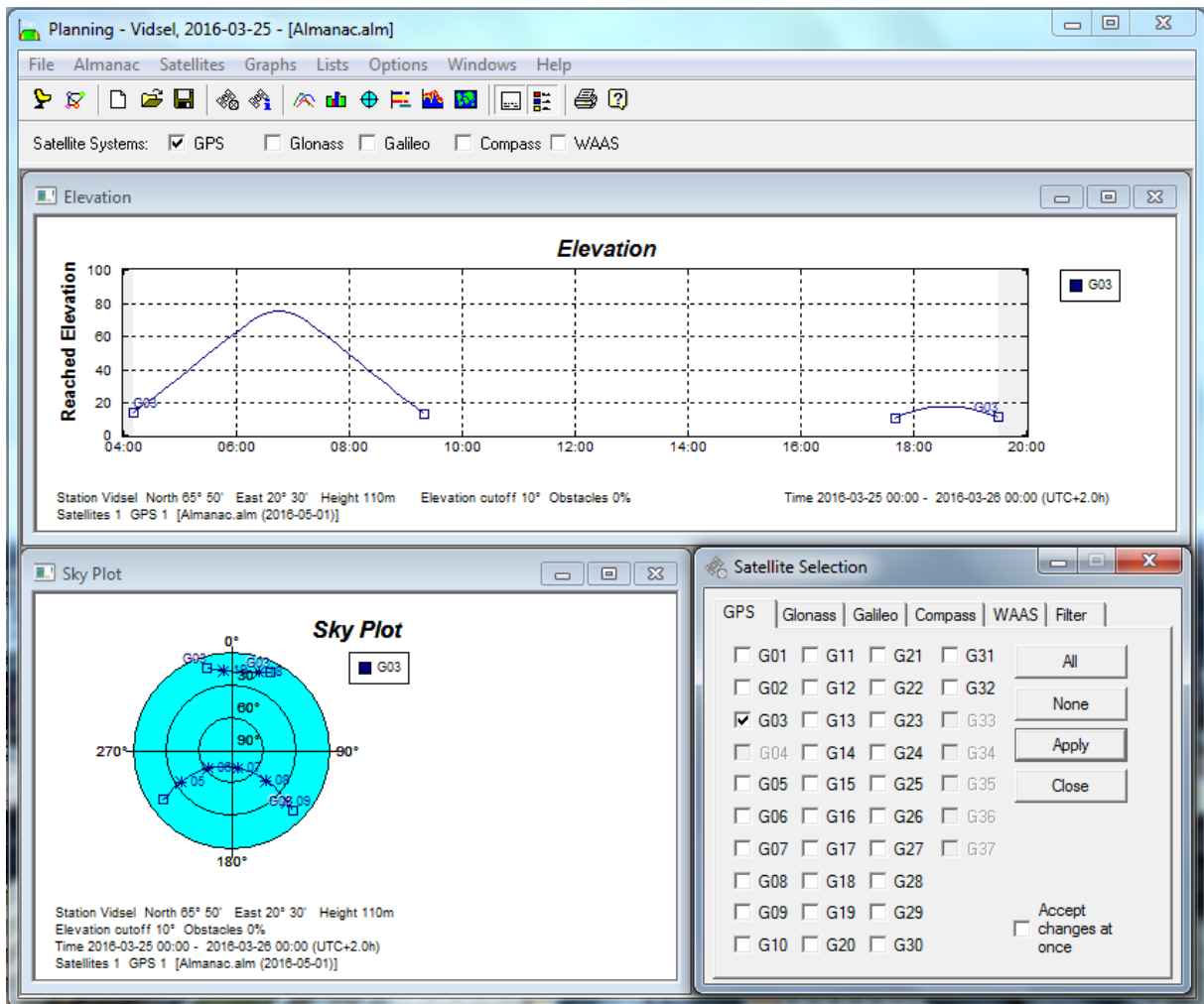


Figure 3.30 Elevation angle and azimuth of satellite G03 for station Vidsel on 25<sup>th</sup> Mar 2016.

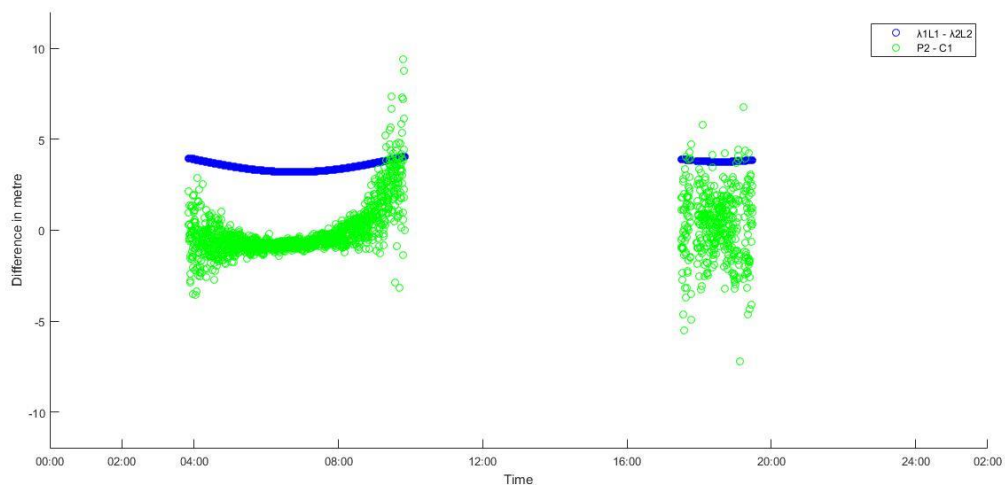


Figure 3.31 Multipath effect on pseudorange and carrier phase observations of satellite G03 for station Vidsel on 25<sup>th</sup> Mar 2016.

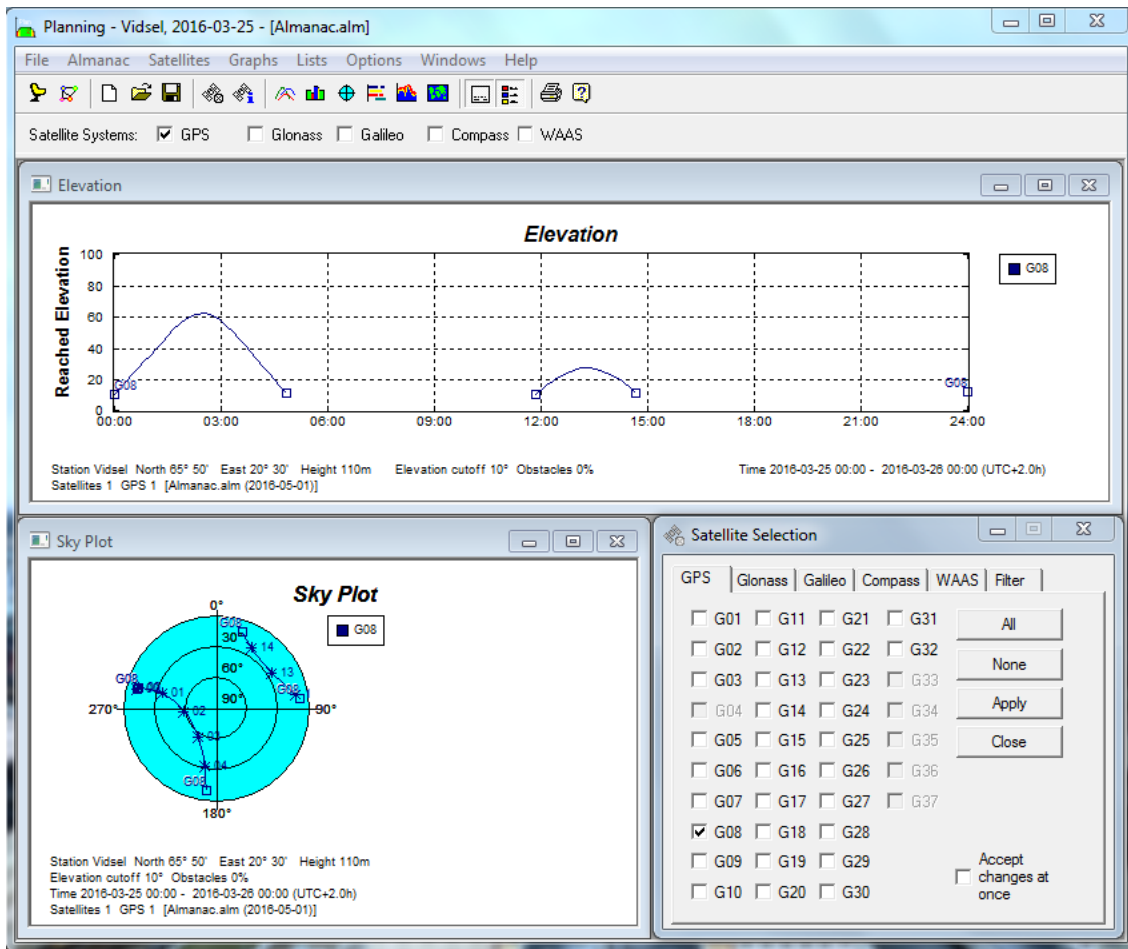


Figure 3.32 Elevation angle and azimuth of satellite G08 for station Vidsel on 25<sup>th</sup> Mar 2016.

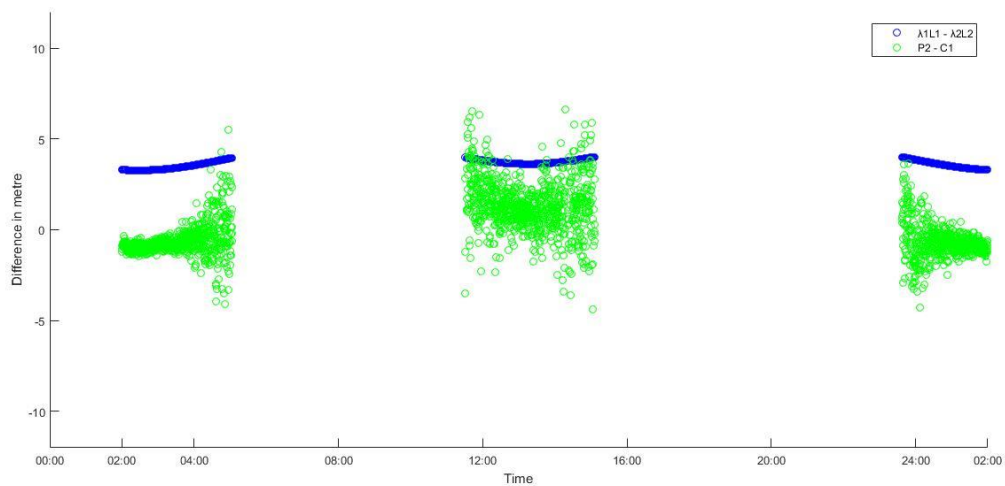


Figure 3.33 Multipath effect on pseudorange and carrier phase observations of satellite G08 for station Vidsel on 25<sup>th</sup> Mar 2016.

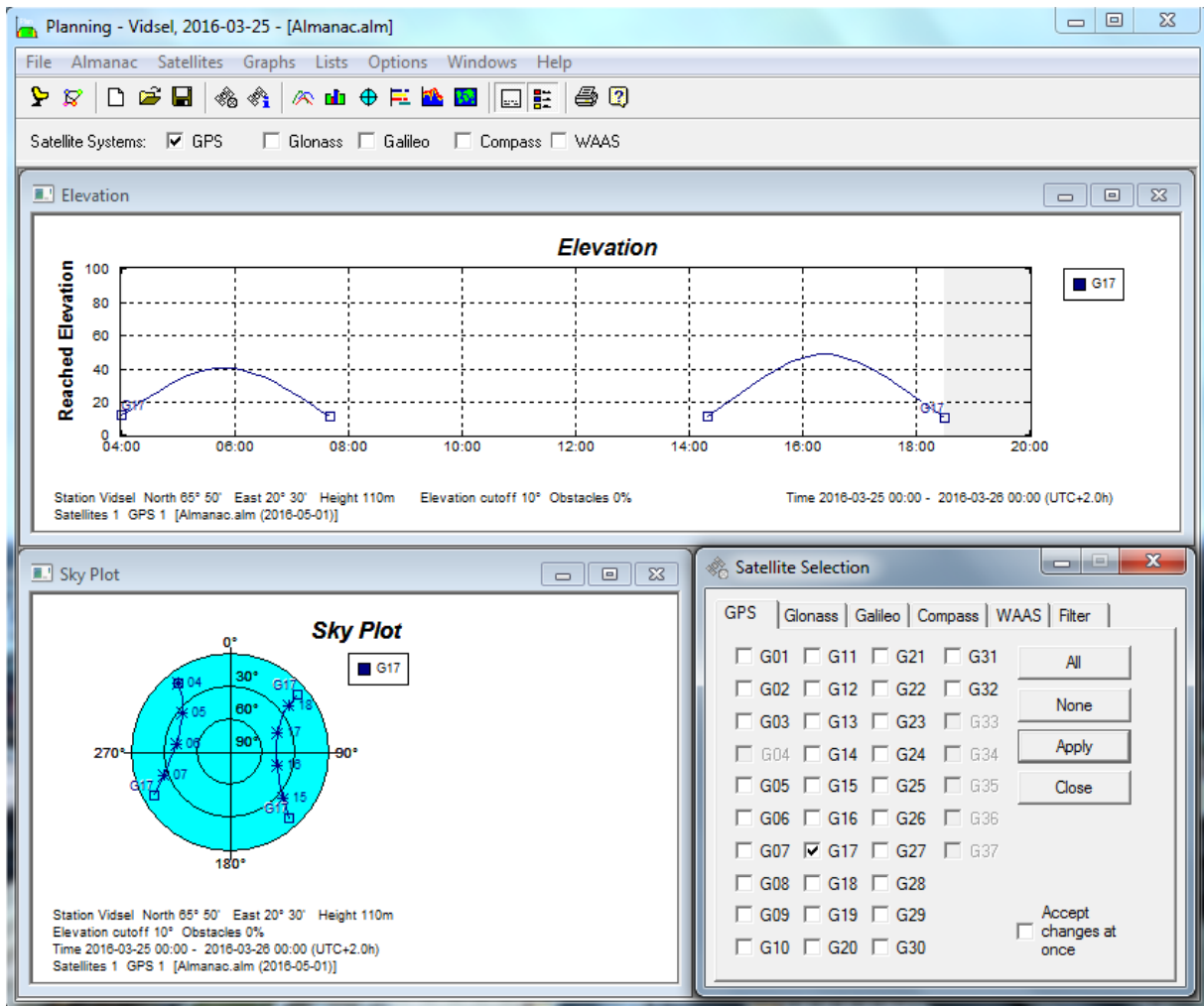


Figure 3.34 Elevation angle and azimuth of satellite G17 for station Vidsel on 25<sup>th</sup> Mar 2016.

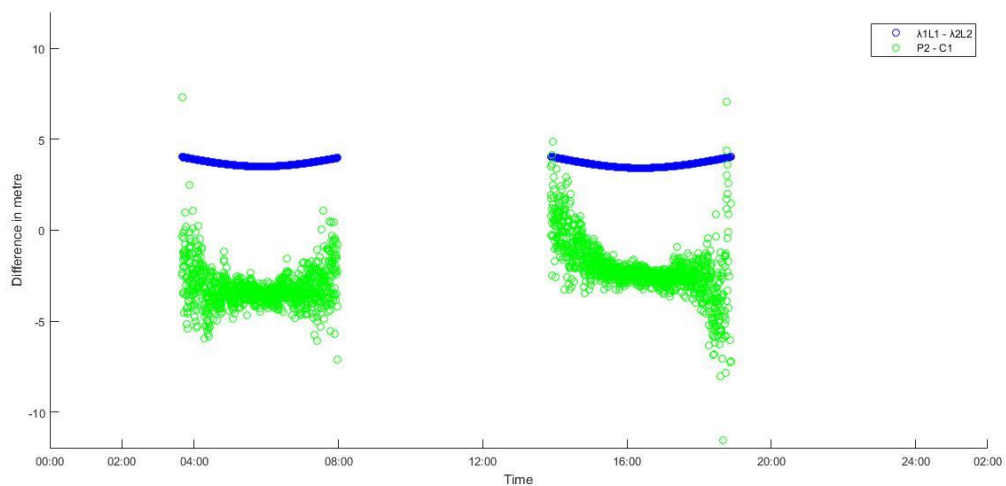


Figure 3.35 Multipath effect on pseudorange and carrier phase observations of satellite G17 for station Vidsel on 25<sup>th</sup> Mar 2016.

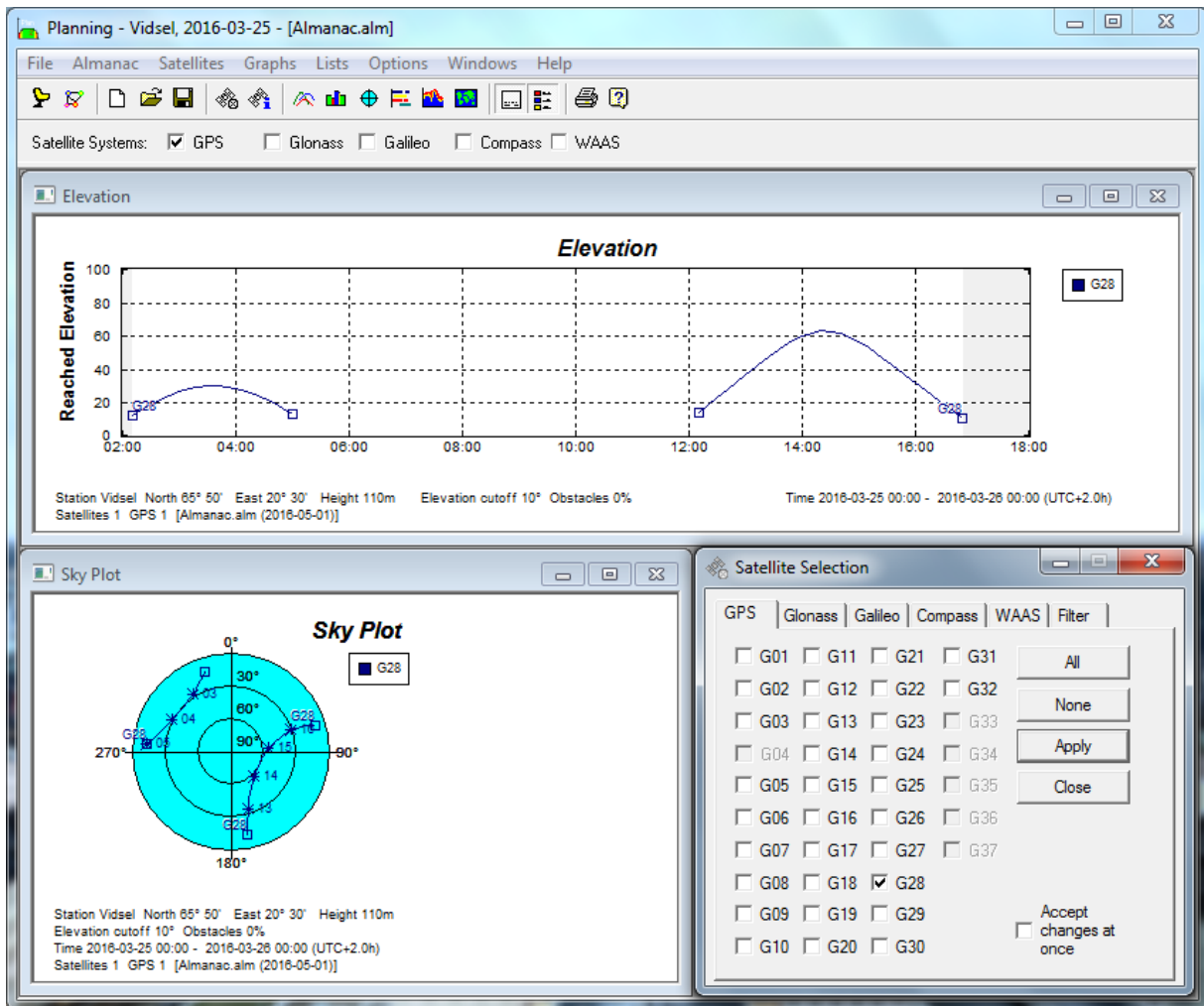


Figure 3.36 Elevation angle and azimuth of satellite G28 for station Vidsel on 25<sup>th</sup> Mar 2016.

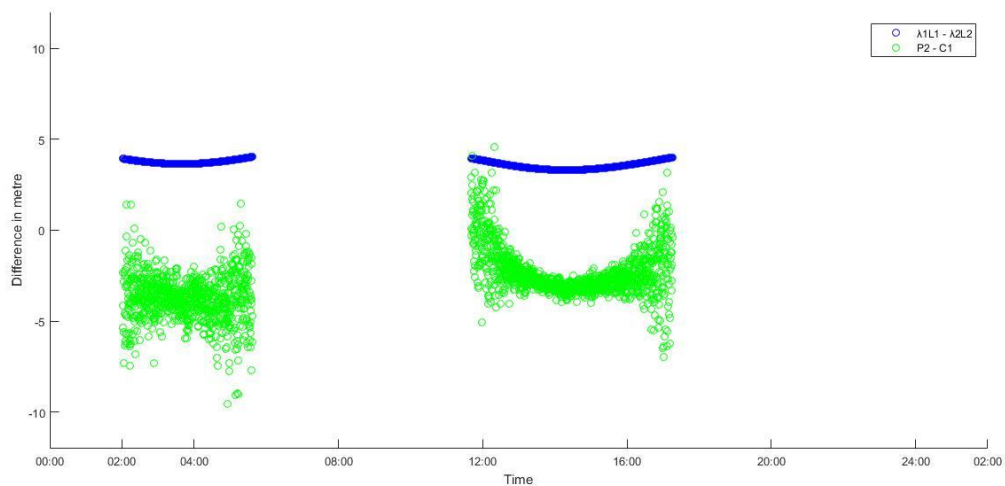


Figure 3.37 Multipath effect on pseudorange and carrier phase observations of satellite G28 for station Vidsel on 25<sup>th</sup> Mar 2016.

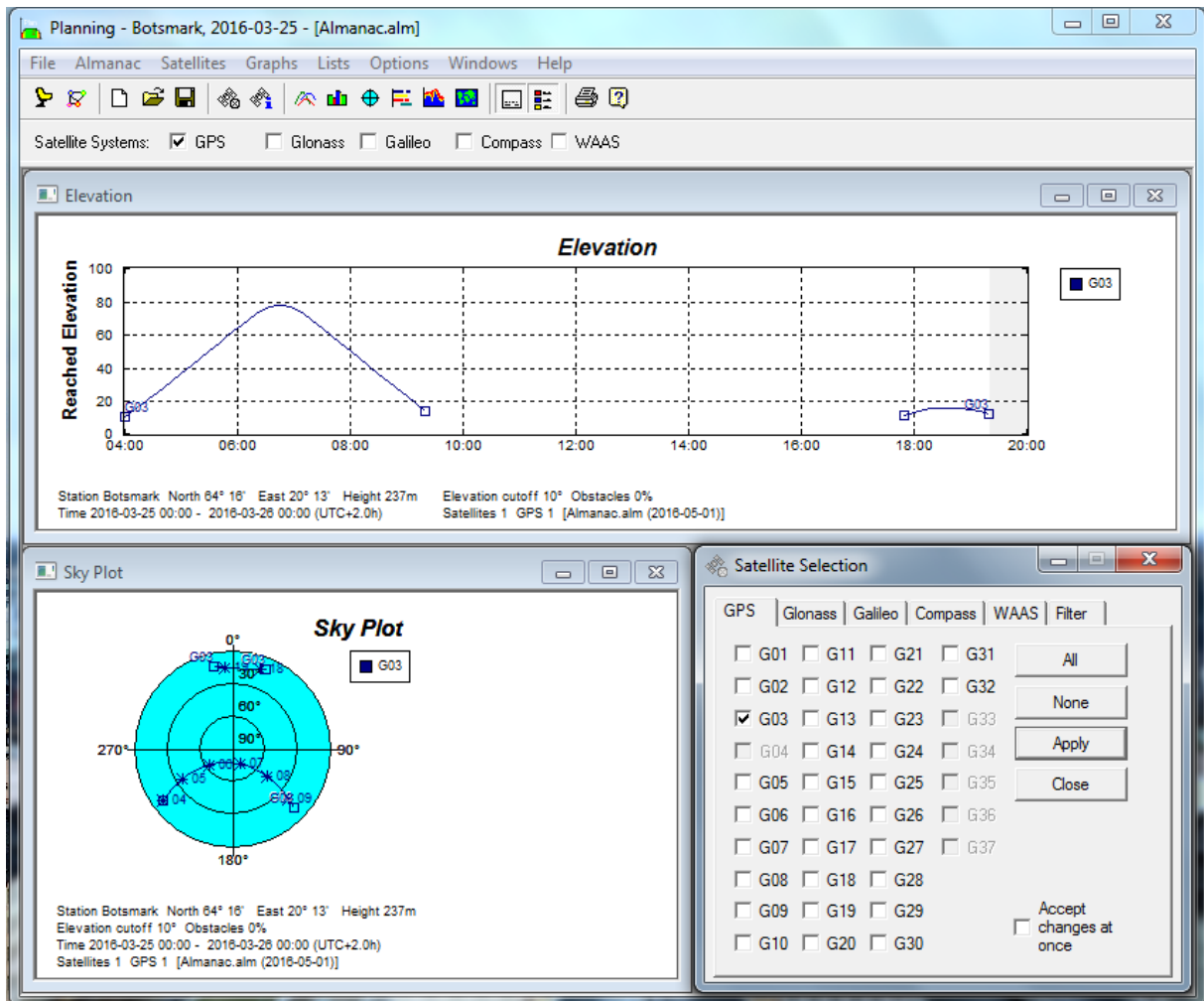


Figure 3.38 Elevation angle and azimuth of satellite G03 for station Botsmark on 25<sup>th</sup> Mar 2016.

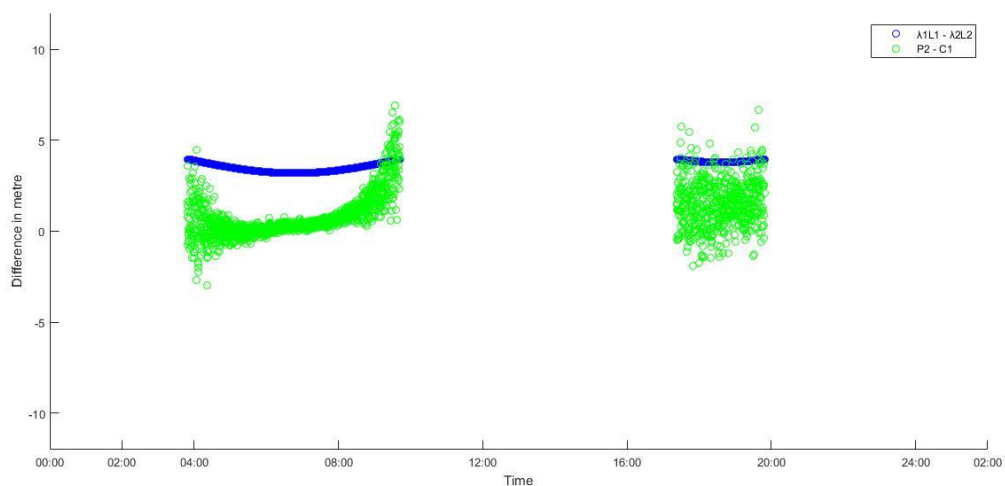


Figure 3.39 Multipath effect on pseudorange and carrier phase observations of satellite G03 for station Botsmark on 25<sup>th</sup> Mar 2016.

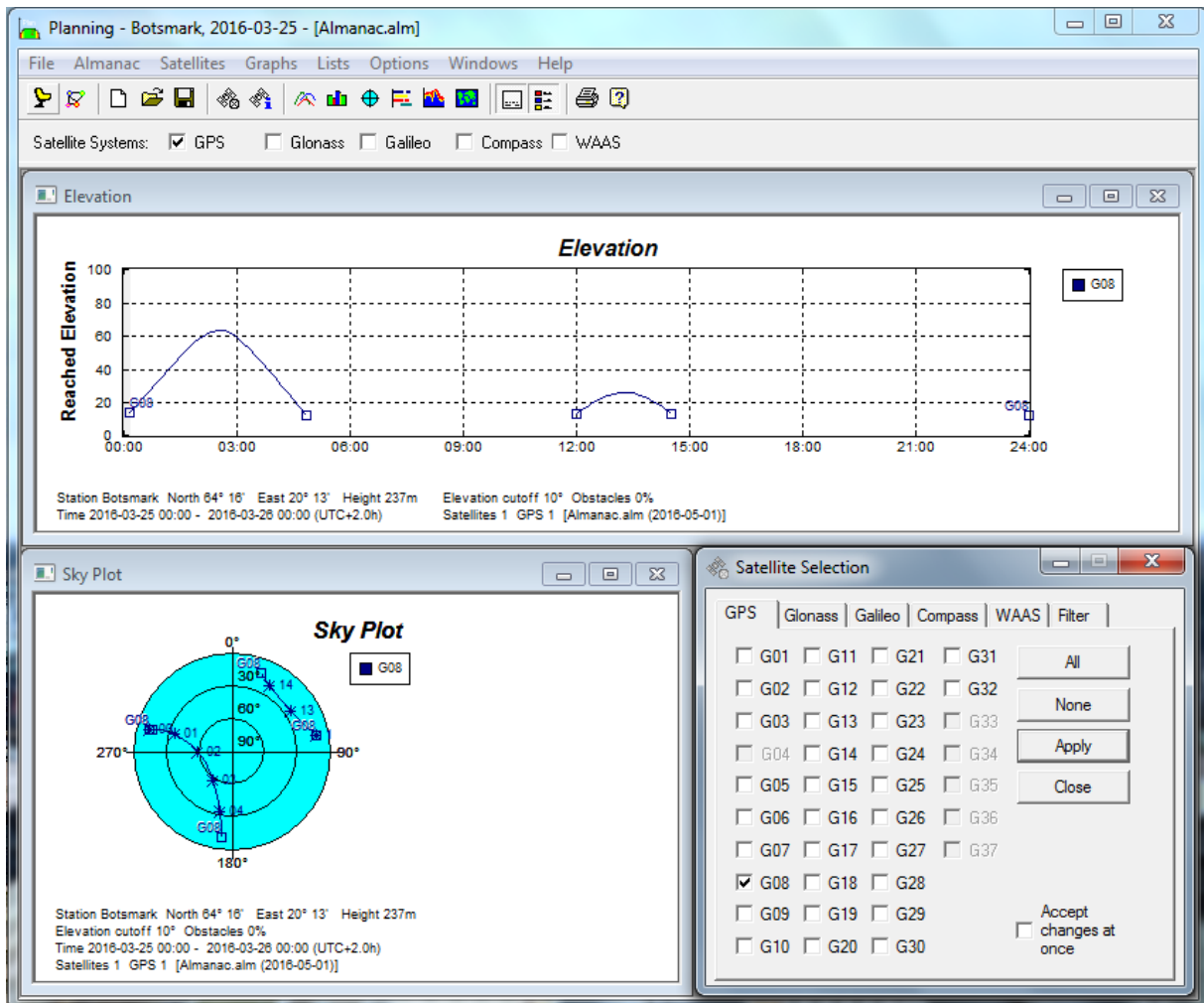


Figure 3.40 Elevation angle and azimuth of satellite G08 for station Botsmark on 25<sup>th</sup> Mar 2016.

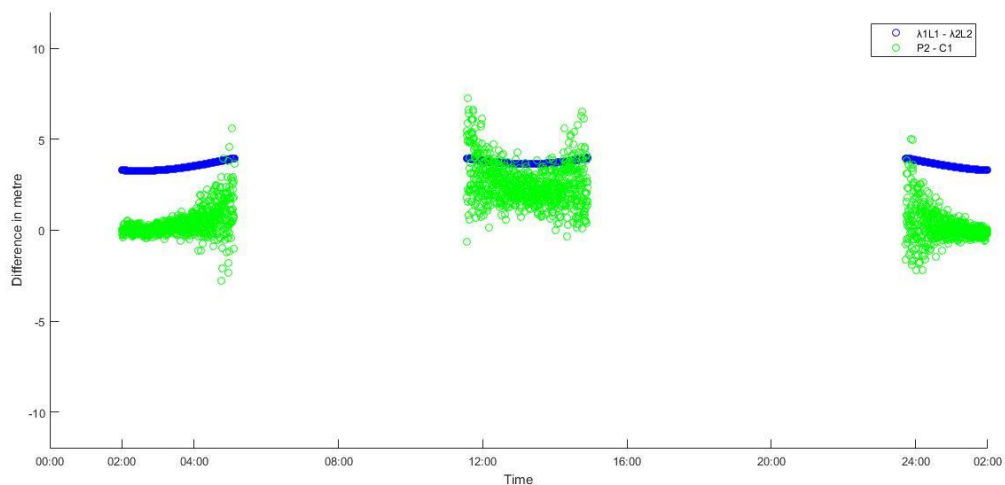


Figure 3.41 Multipath effect on pseudorange and carrier phase observations of satellite G08 for station Botsmark on 25<sup>th</sup> Mar 2016.

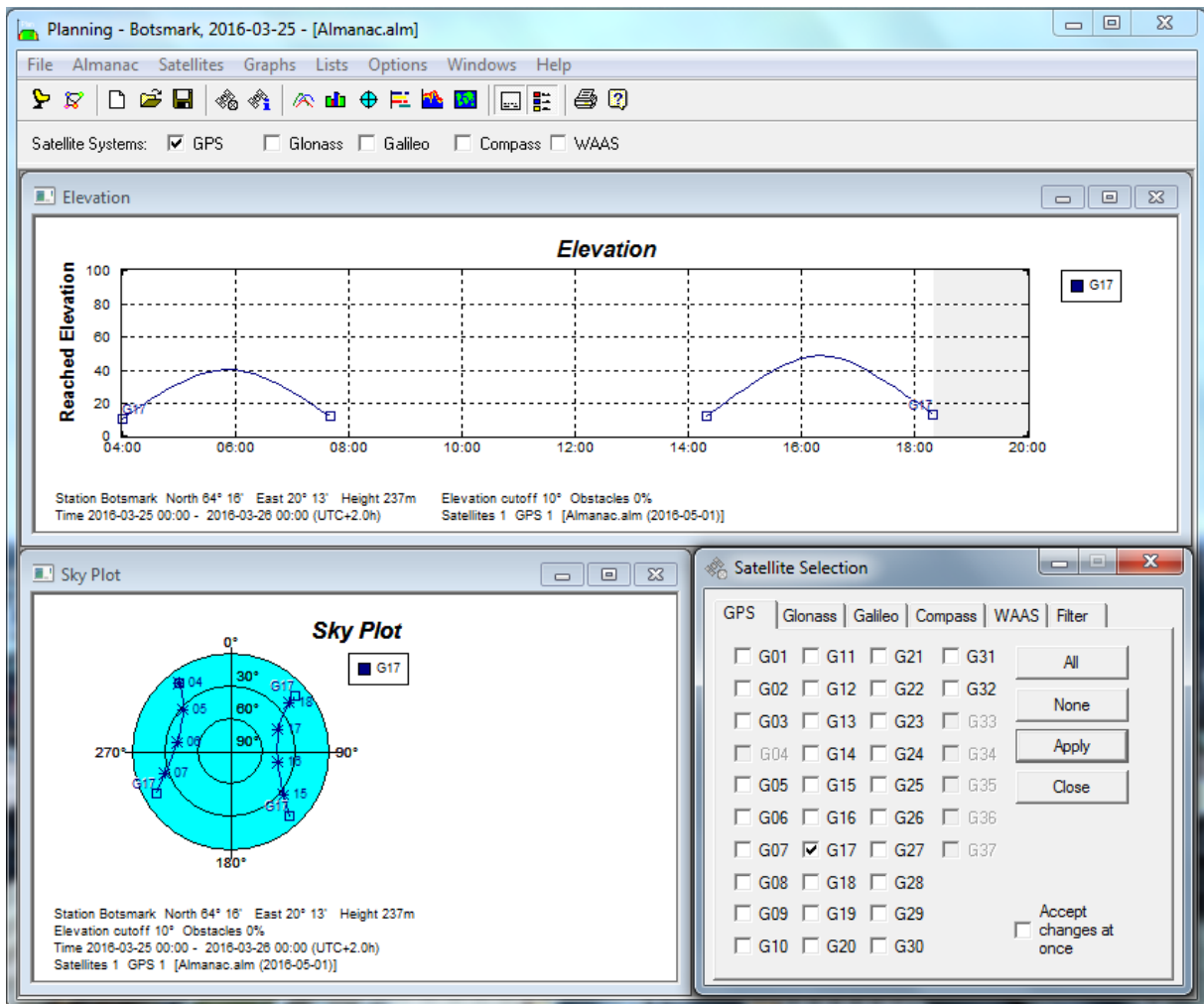


Figure 3.42 Elevation angle and azimuth of satellite G17 for station Botsmark on 25<sup>th</sup> Mar 2016.

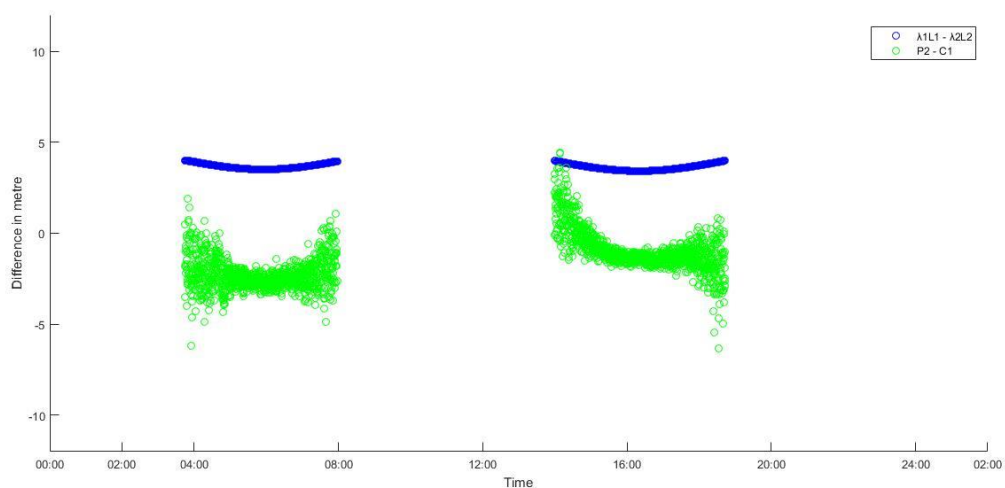


Figure 3.43 Multipath effect on pseudorange and carrier phase observations of satellite G17 for station Botsmark on 25<sup>th</sup> Mar 2016.

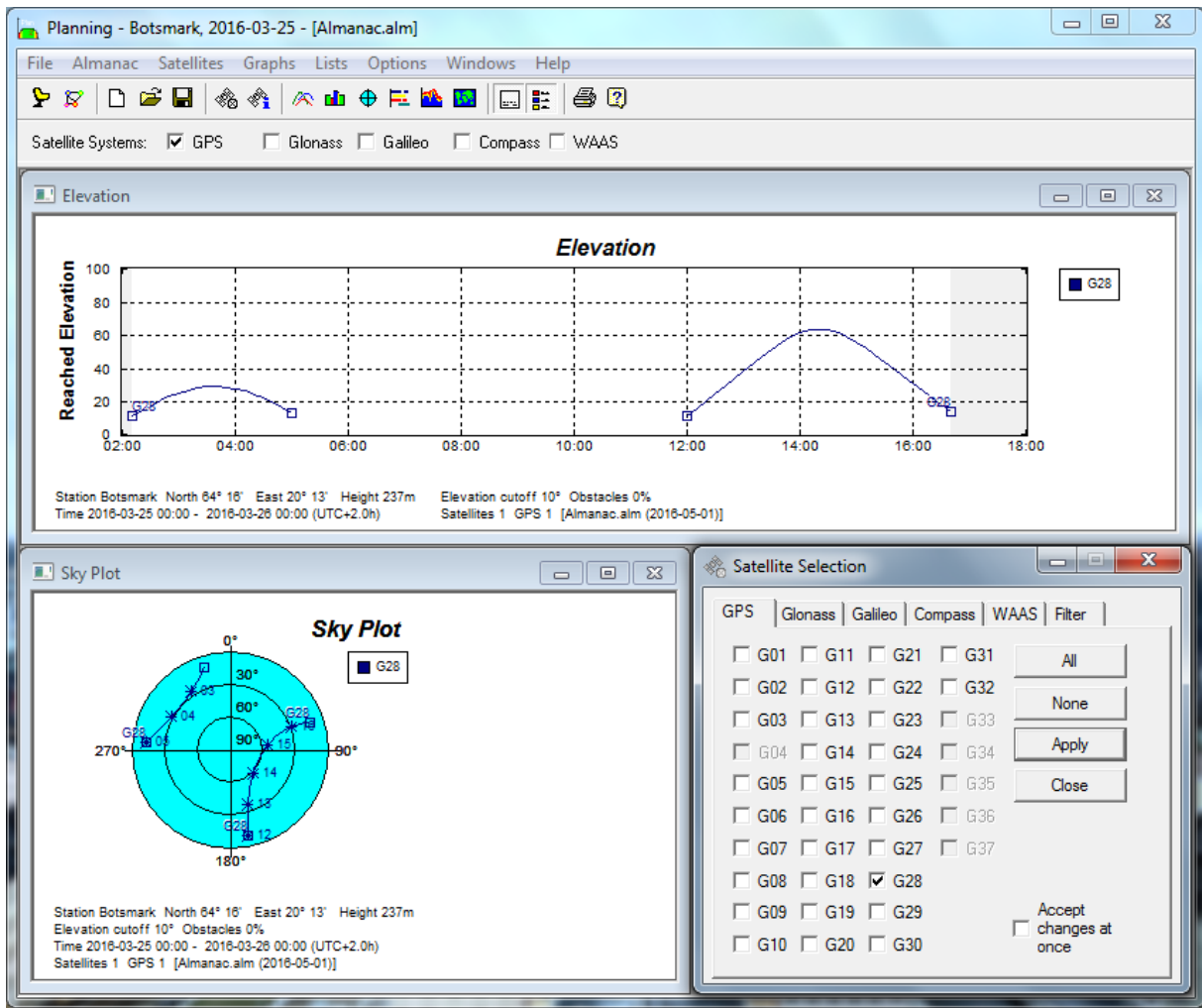


Figure 3.44 Elevation angle and azimuth of satellite G28 for station Botsmark on 25<sup>th</sup> Mar 2016.

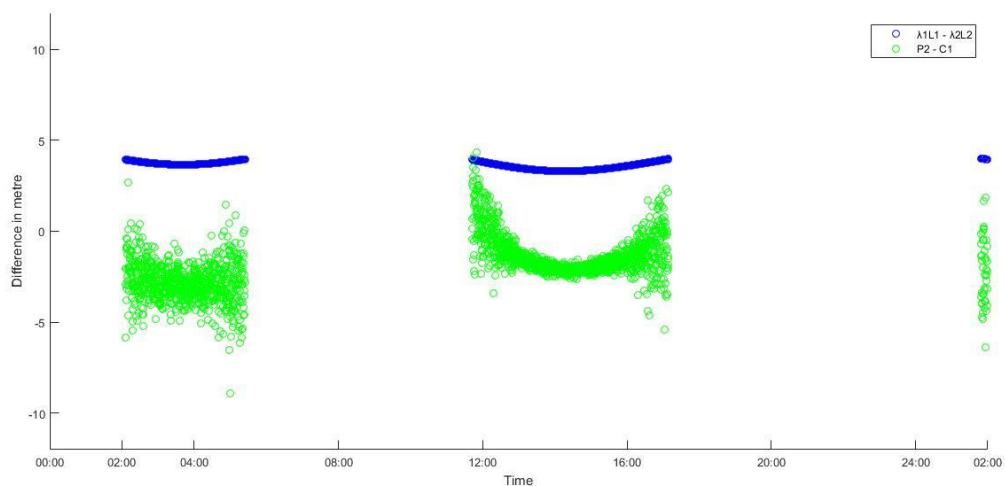


Figure 3.45 Multipath effect on pseudorange and carrier phase observations of satellite G28 for station Botsmark on 25<sup>th</sup> Mar 2016.

## 4. Conclusion and future work

### 4.1 Conclusion for GNSS multipath effect

The focus of this thesis project is the detection and analysis of multipath, which is the dominant error source for most fixed GNSS sites and stations. There are two main methods introduced for the study of multipath errors - Trimble baseline analysis and RINEX analysis. With the experiment of these two methods on SWEPOS station KTH and the application of them on SWEPOS station Vidsel and station Botsmark, the presence of multipath in the GPS satellite signals has been investigated thoroughly; both the overall daily pattern and the detailed selection of certain time period of multipath effect have been examined; and also the effect of multipath on pseudorange code and carrier phase measurements has been differentiated and analysed independently. For the visualization of the results, Trimble baseline analysis has focused on the height of the study station regarding to its reference station over time, on one hand. On the other hand, RINEX analysis has concentrated on the geometry-free combination of pseudorange codes ( $R_{p2} - R_{p1}$ ) and carrier phase measurements ( $\varphi_{L1} - \varphi_{L2}$ ) over time, respectively.

First of all, the multipath effect can be observed for all three stations both from the MATLAB plots made from the output trajectory file from TBC, and from the MATLAB plots created based on the RINEX observation file. As shown in the plots from Trimble trajectory file, the height of the three study stations all has constant fluctuations over time with regard to their own reference station, which indicates that multipath effect does exist in these three stations. The variation of the geometry-free combination of code and carrier measurements displayed in the plots from RINEX observation file is also a sign of multipath errors existing in the satellite signals.

Secondly, the similar daily patterns of the height change of the study station for different days give an intuitive impression of multipath errors. The zoomed-in views of specific time period show in detail that the shapes of different days follow common pattern. All the three study stations share similar results. With quantitative correlation matrix analysis for station KTH and station Vidsel, it is obvious that height values of different days are positively correlated. It is a strong proof that multipath exists in the signal and influences the daily signal constantly to a similar level. RINEX analysis is unable to obtain complete pattern since the single satellite coverage for each station can only be some hours of the day. Therefore, the MATLAB plots for the day are not continuous.

Thirdly, the distinguished analysis for pseudorange code and carrier phase observation has not only proved the existence of multipath errors, and also showed the major difference between these two kinds of observations. It is possible for RINEX analysis since the output observation file contains separate information code and carrier measurements. It is clearly shown in the MATLAB plots that difference in pseudorange codes varied a lot due to the multipath effect. The difference in carrier phase measurements also varied, but it cannot be seen from the plots since it is too minor compared to that in code observations. With the help of the Trimble Planning tool, the elevation angle and the azimuth of each satellite during the day can be observed. It is an important assistance to reach a more comprehensive conclusion. The azimuth can help define the satellite which in the direction facing the multipath signal, if the geometry of the antenna and the surrounding environment are known like station KTH. The satellite with low elevation angle experienced more multipath effect than that with high elevation angle.

## 4.2 Possible future work

Further studies can be conducted if there are opportunities in the future. First of all, I can pay a visit to the two stations – station Vidsel and station Botsmark located up in the northern Sweden. It would be beneficial to the analysis of the result, especially for RINEX analysis. I would be familiar with the mounting of the antenna and the surrounding environment. I would have a clear idea about the relative location of the chimney and the antenna, and thus I could select the satellites more precisely in Trimble Planning tool when conducting RINEX analysis. What's more, I could have a thorough investigation of the surrounding environment to see if there is any other reflective surface or any other factor that could lead to multipath errors. Similar to station KTH, a more intuitive impression on the actual condition of the two stations would make the results more precise and convincing.

As mentioned at the end of Experiment and application section, the different noise level of the pseudorange observations for these two stations can be studied further. One possible cause may be the different types of the receiver and antenna, and this kind of information can be checked in heading of the RINEX observation file. Multipath mitigation could be applied on the settlement of station Botsmark that has lower noise level. One quantitative method to analyse the noise level is to calculate the standard deviation to see how much the data varies from the average.

Another issue that could be paid more attention to is the SNR value. It is the value that indicates the quality of the signal. With the value ranging from 0-9, higher value means better signal quality. Although SNR value for L1 carrier phase observation and that for L2 carrier phase observation are outputs from RINEX observation file, they are not in any use within this thesis project. One possible future work could be combining this value with RINEX analysis. A threshold for good quality could be set, and measurements with value over the threshold could be filtered out. Then the following analysis could be carried out as described in the Method section. It would improve the quality and credibility of the RINEX analysis method to a large extent.

## Reference

- E. Ata, Signal multipath in high precision GPS surveys, *Tehnički Vjesnik* 21(4): 707–713, 2014.
- P. Axelrad, K. Larson, and B. Jones, Use of correct satellite repeat period to characterize and reduce site-specific multipath errors, ION GNSS 18th International Technical Meeting of the Satellite Division, 13-16 September 2005, Long Beach, CA, 2638–2648.
- A. Bilich and K. M. Larson, Mapping the GPS multipath environment using the signal-to-noise ratio (SNR), *Radio Science*, 42, RS6003, 2007, DOI: 10.1029/2007RS003652.
- J. Braun, C. Rocken, and R. Ware, Validation of line-of-sight water vapor measurements with GPS, *Radio Science*, 36(3): 459–472, 2001.
- J. M. Dow, R. E. Neilan, and C. Rizos, The International GNSS Service in a changing landscape of Global Navigation Satellite Systems, *Journal of Geodesy*, 83:191–198, 2009, DOI: 10.1007/s00190-008-0300-3.
- B. Hofmann-Wellenhof, H. Lichtenegger, and E. Wasle, *GNSS - Global Navigation Satellite Systems: GPS, GLONASS, Galileo & more*, SpringerWienNewYork, 2008.
- J. Jakobsen, Kinematic GNSS: Ionospheric variations and characteristics of multipath, Ph.D. thesis, University of Copenhagen, Copenhagen, Denmark, 2010.
- E. D. Kaplan and C. J. Hegarty, *Understanding GPS: principles and applications*, Artech House, 2006.
- K. M. Larson, P. Bodin, and J. Gombert, Using 1 Hz GPS data to measure deformations caused by the Denali fault earthquake, *Science*, 300(5624): 1421–1424, 2003, DOI: 10.1126/science.1084531.
- H. K. Lee and C. Rizos, Position-domain hatch filter for kinematic differential GPS/GNSS, *IEEE Transactions on Aerospace and Electronic Systems*, 44(1): 30-40, 2008, DOI: 10.1109/TAES.2008.4516987.
- R. E. Phelts and P. Enge, The multipath invariance approach for code multipath mitigation, *Proceedings of ION GPS 2000, 13th International Technical Meeting of the Satellite Division of the Institute of Navigation, Salte Lake City, Utah, September 19–22, 2000*: 2376–2384.
- J. K. Ray, M. E. Cannon, and P. C. Fenton, Mitigation of static carrier-phase multipath effects using multiple closely spaced antennas. *Navigation*, 46(3): 193–201, 1999.
- J. Ray and K. Senior, Geodetic techniques for time and frequency comparisons using GPS phase and code measurements, *Metrologia*, 42(4): 215–232, 2003, DOI:10.1088/0026-1394/42/4/005.
- J. M. Tranquilla and J. P. Carr, GPS multipath field observations at land and water sites, *Navigation*, 37(4): 393–414, 1990/91.
- G. E. Vázquez B. and D. A. Grejner-Brzeziska, A case of study for Pseudorange multipath estimation and analysis: TAMDEF GPS network, *Geofísica Internacional* 51(1): 63–72, 2012.

# Reports in Geodesy and Geographic Information Technology

The TRITA-GIT Series - ISSN 1653-5227

- 16-001 **Marvin McCutchan.** Investigation of Geoid Changes in Northern Europe Using Latest Data from the Dedicated Satellite Gravity Mission GRACE. Master of Science thesis in Geodesy No. 3141. Supervisor: Huaan Fan. January 2016.
- 16-002 **Alice Tourtier.** Study of the contribution of an ionospheric model embedded on a dual frequency receiver. Master of Science thesis in Geodesy No. 3142. Supervisors: Anna Jensen (KTH), Marion Aubault and Sebastien Rougerie (CNES). February 2016.
- 16-003 **Shinan Wang.** Detection and Analysis of GNSS Multipath. Master of Science thesis in Geodesy No. 3143. Supervisor: Anna Jensen. June 2016.

TRITA-GIT EX 16-003  
ISSN 1653-5227  
ISRN KTH/GIT/EX--16/003-SE

TRITA TRITA-GIT EX 16-003  
ISSN 1653-5227